AFRL-ML-WP-TM-2007-4019

INFLUENCE OF SURFACE ROUGHNESS ON THE SPECULAR REFLECTANCE OF LOW GLOSS COATINGS USING BIDIRECTIONAL REFLECTANCE MEASUREMENTS

Lisa M. Farrier

Nonstructural Materials Branch (AFRL/MLBT)
Nonmetallic Materials Division
Materials and Manufacturing Directorate
Air Force Research Laboratory
Air Force Materiel Command
Wright-Patterson Air Force Base, OH 45433-7750

OCTOBER 2006

Thesis

Approved for public release; distribution unlimited.

STINFO COPY

MATERIALS AND MANUFACTURING DIRECTORATE
AIR FORCE RESEARCH LABORATORY
AIR FORCE MATERIEL COMMAND
WRIGHT-PATTERSON AIR FORCE BASE, OH 45433-7750

NOTICE AND SIGNATURE PAGE

Using Government drawings, specifications, or other data included in this document for any purpose other than Government procurement does not in any way obligate the U.S. Government. The fact that the Government formulated or supplied the drawings, specifications, or other data does not license the holder or any other person or corporation; or convey any rights or permission to manufacture, use, or sell any patented invention that may relate to them.

This report was cleared for public release by the Air Force Research Laboratory Wright Site (AFRL/WS) Public Affairs Office and is available to the general public, including foreign nationals. Copies may be obtained from the Defense Technical Information Center (DTIC) (http://www.dtic.mil).

AFRL-ML-WP-TM-2007-4019 HAS BEEN REVIEWED AND IS APPROVED FOR PUBLICATION IN ACCORDANCE WITH ASSIGNED DISTRIBUTION STATEMENT.

*//Signature//

LISA M. FARRIER, Program Manager
Nonstructural Materials Branch
Nonmetallic Materials Division

//Signature//

STEPHEN L. SZARUGA, Acting Chief
Nonstructural Materials Branch
Nonmetallic Materials Division

//Signature//

SHASHI K. SHARMA, Acting Deputy Chief
Nonmetallic Materials Division
Materials and Manufacturing Directorate

This report is published in the interest of scientific and technical information exchange, and its publication does not constitute the Government's approval or disapproval of its ideas or findings.

*Disseminated copies will show "//signature//" stamped or typed above the signature blocks.

REPORT DOCUMENTATION PAGE

Form Approved
OMB No. 0704-0188

1. REPORT DATE *(DD-MM-YY)*	2. REPORT TYPE	3. DATES COVERED *(From - To)*
October 2006	Thesis	

4. TITLE AND SUBTITLE
INFLUENCE OF SURFACE ROUGHNESS ON THE SPECULAR REFLECTANCE OF LOW GLOSS COATINGS USING BIDIRECTIONAL REFLECTANCE MEASUREMENTS

5a. CONTRACT NUMBER
In-house

5b. GRANT NUMBER

5c. PROGRAM ELEMENT NUMBER
62102F

6. AUTHOR(S)
Lisa M. Farrier

5d. PROJECT NUMBER
M06R

5e. TASK NUMBER
20

5f. WORK UNIT NUMBER
00

7. PERFORMING ORGANIZATION NAME(S) AND ADDRESS(ES)
Nonstructural Materials Branch (AFRL/MLBT)
Nonmetallic Materials Division
Materials and Manufacturing Directorate
Air Force Research Laboratory, Air Force Materiel Command
Wright-Patterson Air Force Base, OH 45433-7750

8. PERFORMING ORGANIZATION REPORT NUMBER
AFRL-ML-WP-TM-2007-4019

9. SPONSORING/MONITORING AGENCY NAME(S) AND ADDRESS(ES)
Materials and Manufacturing Directorate
Air Force Research Laboratory
Air Force Materiel Command
Wright-Patterson AFB, OH 45433-7750

10. SPONSORING/MONITORING AGENCY ACRONYM(S)
AFRL-ML-WP

11. SPONSORING/MONITORING AGENCY REPORT NUMBER(S)
AFRL-ML-WP-TM-2007-4019

12. DISTRIBUTION/AVAILABILITY STATEMENT
Approved for public release; distribution is unlimited.

13. SUPPLEMENTARY NOTES
This final report is a Master of Materials Science and Engineering dissertation submitted to the University of Dayton in partial fulfillment of its requirements for a Masters degree.

PAO Case Number: AFRL/WS 06-2665, 13 Nov 2006. Report contains color.

14. ABSTRACT (*Maximum 200 words*)
The objective of this study was to determine the effects of surface roughness and incident angle on the reflectance of low gloss coatings at grazing incidence. A specular peak has been identified from the forward scatter at longer wavelengths, 3.39 μm and 10.6 μm, for various painted surfaces. Depending on the surface roughness and wavelength, this specular component occurs at different angles. However, this effect has not been observed in the visible region. Material surfaces with well characterized surface roughness have been measured at a wavelength of 0.633 μm in an attempt to observe this effect in the visible region. The angle at which it was observed for various roughnesses has been obtained using bidirectional reflectance distribution function (BRDF) measurements.

15. SUBJECT TERMS
Reflectance, coatings, specular, wavelength bidirectional reflectance distribution function (BRDF)

16. SECURITY CLASSIFICATION OF:			17. LIMITATION OF ABSTRACT:	18. NUMBER OF PAGES	19a. NAME OF RESPONSIBLE PERSON (Monitor)
a. REPORT	b. ABSTRACT	c. THIS PAGE			Lisa M. Farrier
Unclassified	Unclassified	Unclassified	SAR	74	19b. TELEPHONE NUMBER *(Include Area Code)* N/A

Standard Form 298 (Rev. 8-98)
Prescribed by ANSI Std. Z39-18

TABLE OF CONTENTS

LIST OF ILLUSTRATIONS

LIST OF TABLES

ABSTRACT

INFLUENCE OF SURFACE ROUGHNESS ON THE SPECULAR REFLECTANCE OF LOW GLOSS COATINGS USING BIRDIRECTIONAL REFLECTANCE MEASUREMENTS

Farrier, Lisa Marie
University of Dayton

Advisor: Dr. Andrey Voevodin

The objective of this study was to determine the effects of surface roughness and incident angle on the reflectance of low gloss coatings at grazing incidence. A specular peak has been identified from the forward scatter at longer wavelengths, 3.39 μm and 10.6 μm, for various painted surfaces. Depending on the surface roughness and wavelength, this specular component occurs at different angles. However, this effect has not been observed in the visible region. Material surfaces with well characterized surface roughness have been measured at a wavelength of 0.633 μm in an attempt to observe this effect in the visible region. The angle at which it was observed for various roughnesses has been obtained using bidirectional reflectance distribution function (BRDF) measurements.

ACKNOWLEDGEMENTS

My special thanks to my advisor, Andrey Voevodin, for undertaking a project outside of his research area. Bill Lynn for opening his door every time I had a question and helping me interpret the data.

I would also like to thank Joel Johnson for his coatings formulation experience and assistance in sample preparation. Wendy Shemano for her patience and expertise in operating the scatterometers. Thanks to Steve Szaruga for guidance in determining a project to pursue and allowing me the time to complete this project. Art Safriet for precision machining the sample mounts in order to balance and spin the panels. Mark Webb for helping design the sample mount. John Buhrmaster for access to the spray booth on multiple occasions. Carl Hager for training me on the Wyko interferometer.

And, finally to all my office mates who had to listen to all the obstacles encountered during this project.

CHAPTER ONE

INTRODUCTION

Low visibility is essential for all military aircraft. To achieve low visibility, the surface of a military airplane must scatter rather than reflect light, thus, requires coatings that have a very matte finish, or extremely low gloss. Military aircraft are also colored to match the predominant colors of the surrounding environment. An airplane flying at low to medium altitudes is easily sighted against the bright background of the daytime sky. As a result, military aircraft are typically painted a shade of gray. The combination of color and gloss effectively reduces the range at which an airborne object becomes visible.

Military coating systems are comprised of a conversion coating, primer, and topcoat as shown in Figure 1. It is, however, the responsibility of the topcoat to provide both the low gloss properties and proper color. The low visual gloss feature requires that the topcoat contains a high pigment volume concentration (PVC) of inorganic pigments and flatting agents in order to produce a rough uneven surface. In addition, tinting pigments such as titanium dioxide and carbon black are incorporated in the topcoat to produce the gray color. A color difference of less than 1 when compared to the specified color chip in FED-STD-595 [1] is required. Long term durability and

fluid resistance is achieved using aliphatic polyurethanes as the binder. Details of the organic coating chemistry are provided elsewhere [2].

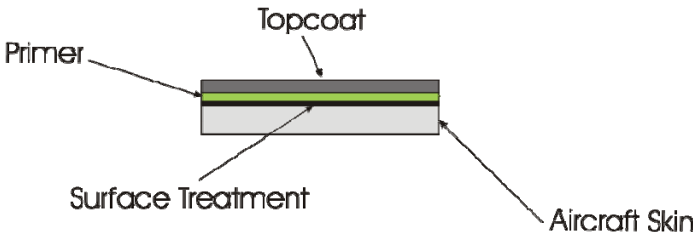

Figure 1. Generic military coating arrangement.

Currently, a handheld gloss measurement tool is used to determine the coating's ability to provide visual camouflage. The U.S. Department of Defense specification number for standard MIL-PRF-85285 [3] polyurethane topcoat requires a specular gloss of less than 5 gloss units at 60 degrees angle of incidence and less than 9 gloss units at 85 degrees. However, a coating with a gloss less than 5 gloss units is so highly pigmented that it lacks durability and becomes difficult to clean. One would question whether these coatings are being over specified at the expense of durability. Thus, the purpose of this study is to better understand the scatter behavior of low gloss coatings with respect to their specified requirements.

Because glossmeters are limited by specific angles of incidence, bidirectional reflectance is a more appropriate technique to characterize the scatter behavior of these materials. Bidirectional reflectance is a common technique that is used to quantify the scatter properties of materials as a

function of wavelength and incident angle. Prior measurements (see Figure 2 and Figure 3) of like coatings have revealed a specular reflection component at longer wavelengths, 3.39 μm and 10.6 μm. This specular component was observed to occur at different angles depending on the surface roughness and wavelength. Also, longer wavelengths appeared to produce this effect at smaller angles of incidence, thus, it is expected that shorter visible wavelengths would produce this effect at grazing angles (from 70 to 88 degrees) of incidence. However, this effect has not been observed in the visible region indicating that the current camouflage coatings may be over specified.

Figure 2 is a plot of the bidirectional reflectance distribution function (BRDF) of a generic painted surface at a wavelength of 10.6 μm exhibiting specular behavior for all angles of incidence. At the shorter 3.39 μm wavelength, specular peaks are not revealed until approaching 75 degrees angle of incidence as shown in Figure 3.

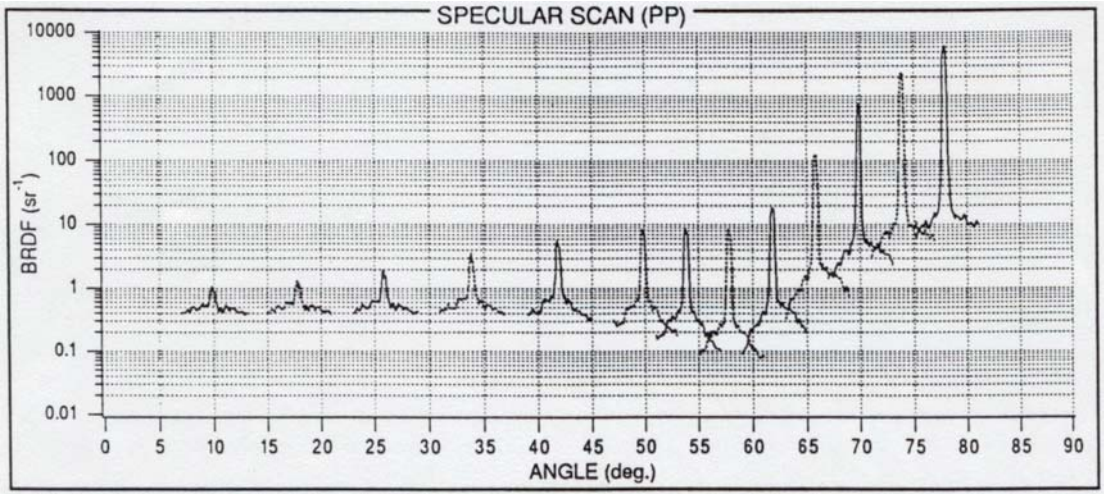

Figure 2. BRDF plot at a wavelength of 10.6 μm.

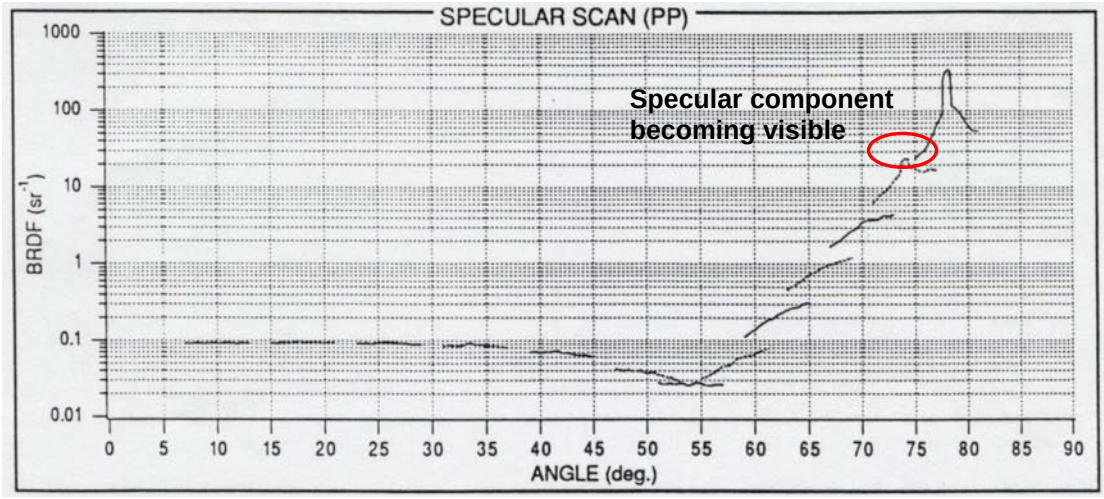

Figure 3. BRDF plot at a wavelength of 3.39 μm.

The objective of this study was to determine the effects of surface roughness and incident angle on the specular reflectance of low gloss coatings in the visible region. Material surfaces were created with well characterized surface roughness and measured at a wavelength of 0.633 μm

in an attempt to observe this effect in the visible. The angle at which it was observed for various roughnesses was obtained using BRDF.

CHAPTER TWO

BACKGROUND AND THEORY

Reflection of Light

Light incident upon a surface can be reflected, absorbed, or transmitted. The interaction depends on the physical characteristics of the light as well as the physical composition and characteristics of the object. The conservation of energy leads to the following equation:

$$E_r + E_t + E_a = 1,$$

where E_r is the light reflected back from the surface of the object, E_t is the light transmitted through the object, and E_a is the light absorbed by the object. Each is a function of wavelength. Thus, reflected waves are simply those that are neither transmitted nor absorbed. The law of reflection states that light will be reflected from a surface at an angle equal to the incident angle, $\theta_r = \theta_i$, which is called specular reflection. Both angles are typically measured with respect to the normal to the surface as shown in Figure 4. The law applies to the reflection of light from surfaces that are horizontal, vertical, angled, and/or curved.

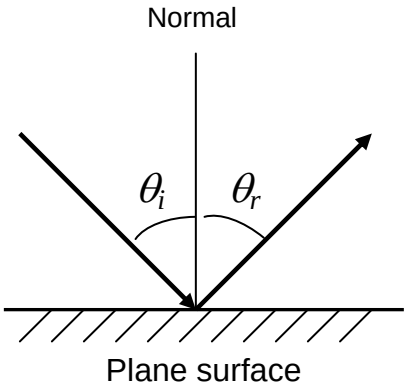

Figure 4. Law of reflection.

The reflection may be specular or diffuse depending on the nature of the surface as illustrated in Figure 5 [4]. For smooth objects such as mirrors, light strikes the surface and is reflected in a single direction following the law of reflection as shown in Figure 5(a). A Lambertian surface or surface with perfectly matte properties results in diffuse reflection with light being reflected from the surface equally in all directions as shown in Figure 5(b). Most objects, however, exhibit some combination of mixed reflection as shown in Figure 5(c) where there is both a coherent component of specular reflection and a diffuse or incoherent scattering component present. In paint terms, the various distributions of reflected light are referred to as gloss, matte, and semi-gloss finishes, respectively. The more evenly the intensity is distributed in all directions, the less glossy a surface will appear.

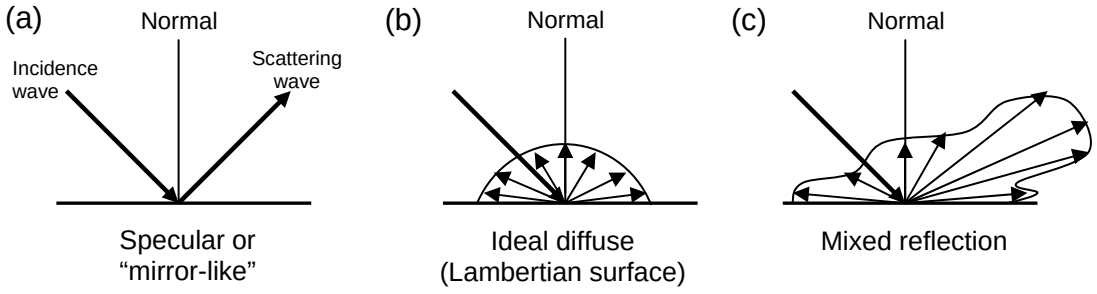

Figure 5. Reflection models.

Surface scatter is also dependent upon the relationship between the wavelength of electromagnetic radiation and surface roughness. A surface behaves as a smooth surface as long as the surface variations are very small relative to the wavelength of the incident light as defined by the Rayleigh criterion. But, if the irregularities on the surface of an object are larger than the wavelength of light, the surface behaves as a rough or matte surface. More information on this subject may be found in Stover [5].

Gloss and Surface Roughness

Gloss is the ability of a surface to reflect light into the specular direction [6]. It is proportional to the reflectance of the surface. The reflection is given by the Fresnel equation which is dependent on the angle of incidence and the difference between the refractive indices.

The gloss level is primarily influenced by surface roughness. Gloss and surface roughness share a linear relationship, hence, the lower the gloss,

the higher the surface roughness. For a paint or coating, pigmentation is used to vary the surface roughness in an attempt to control the gloss. The protrusion of these pigment particles causes the reflected light to be scattered resulting in low gloss. It is affected by several factors including pigment particle size, shape, and concentration. Figure 6 depicts the typical microstructure of a military coating system. The image shows that the topcoat is highly pigmented with an assortment of particles of varying shapes and sizes. Due to the high PVC, these coatings contain a smaller amount of polymeric resin to wet out the pigments and fillers compared to high gloss coatings. The lower binder content inherently provides less durability as described below.

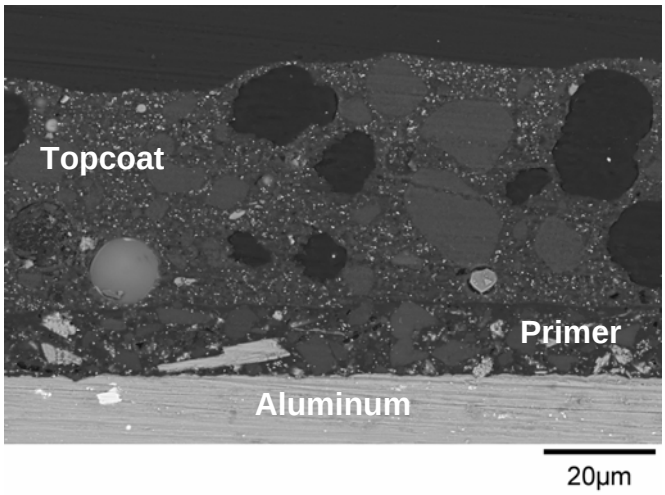

Figure 6. Topcoat pigment representation.

Low gloss can be achieved through the use of pigmentation, but not without the reduction of various coating properties. The relative change in coating properties as a result of increasing PVC is shown in Figure 7 [7]. At high pigment loadings, porosity leads to the loss of barrier properties and corrosion protection. Catastrophic loss occurs at the critical pigment volume concentration (CPVC). The CPVC is the point at which there is not enough polymeric resin to level out the surface. At the CPVC, the maximum number of particles is present at the surface without breaking through the polymer corresponding to the onset of surface roughness [8]. It should not be confused with the point of maximum surface roughness.

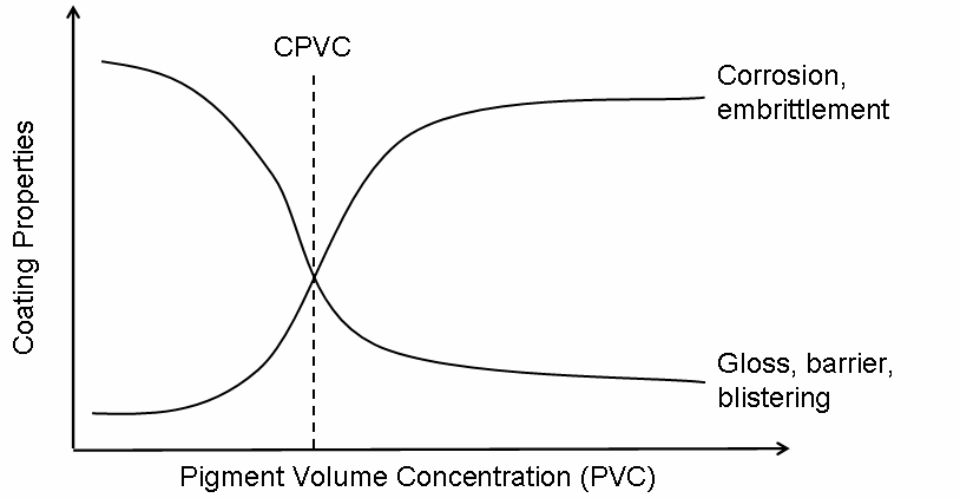

Figure 7. Effects of pigment loading.

Gloss is measured using a glossmeter. It is determined by measuring the percent reflectance using a simple photodetector arranged so that the illumination and detection occurs at equal and opposite angles as illustrated in Figure 8. Measurements are given by a numerical value that relates the amount of specular reflection to that of a standard surface under the same geometric conditions. The standard surface is polished black glass with a refractive index of 1.567. Thus, the measurements can only be used for comparison purposes. The test method is defined by the ASTM standard D523 [9].

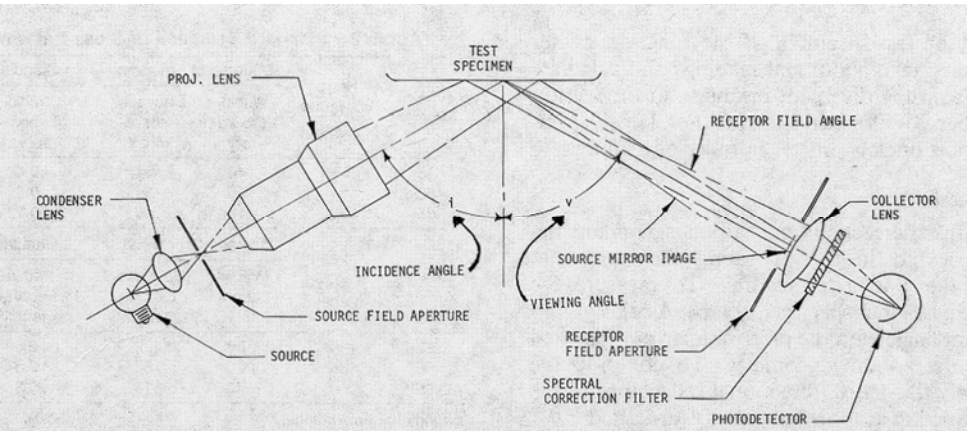

Figure 8. Glossmeter design.

Meters are configured to operate at three different illumination angles 60, 20 and 85 degrees. The most common angle for gloss measurement is 60 degrees. The 60 degree geometry is used as a good general evaluation of gloss with a linear range between 10 and 70 gloss units as shown in Figure 9

[10]. However, it becomes nonlinear at the two extremes requiring other measurement geometries to be used to improve resolution for matte and glossy surfaces. The intensity derived from the Fresnel equation increases as the angle of incidence increases. It is at its greatest for angles of incidence nearly parallel to the mean of that surface. Therefore, the 85 degree geometry is more applicable for surfaces with 60 degree gloss values less than 10. The 20 degree geometry is most often used for surfaces with 60 degree gloss values greater than 70 or high gloss.

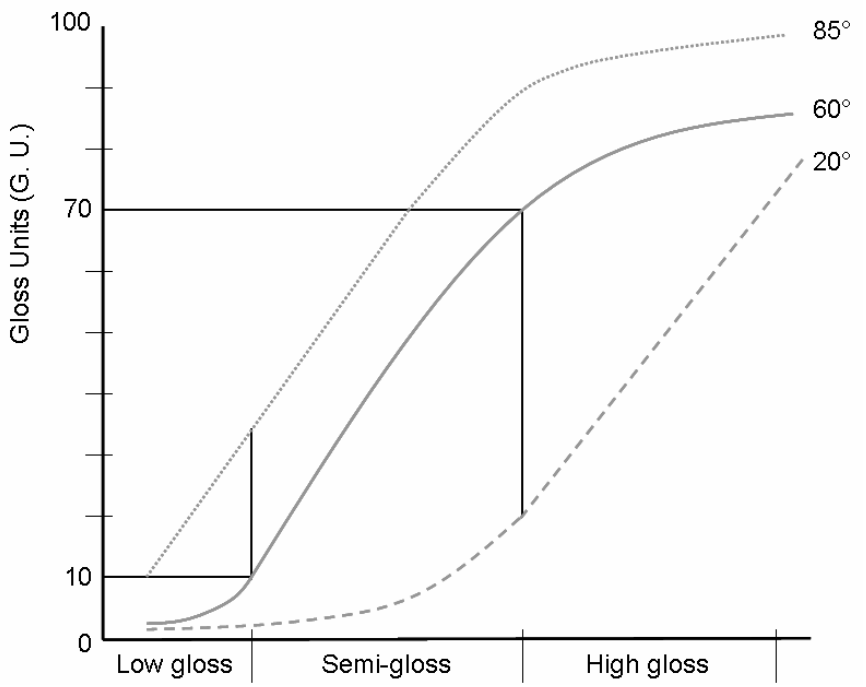

Figure 9. Determination of gloss measurement geometries.

The measurement results are also influenced by the calibration of the instrument and the type of measuring instrument. Measurement readings

may vary due to mistakes performed during calibration such as using a dirty or damaged calibration standard. The type of instrument also affects the measurement results. Inconsistencies have been observed for measurements taken at the same angle using two different meters. Often two different gloss values are produced although meters are manufactured to conform to the same gloss standard. Arney et. al. [11] determined that the acceptance angle is different depending on manufacturer and that the difference of only a few tenths of a degree can significantly alter the gloss readings produced by an instrument.

Bidirectional Reflectance

BRDF is a commonly accepted measurement technique used to describe the distribution of reflected light at a surface. The bidirectional distribution function is determined from the ratio of scattered surface radiance divided by incident surface irradiance at some specified polar (θ) and azimuthal angles (ϕ). BRDF is typically presented as a function of wavelength. The following equation was first defined by Nicodemus [12].

$$BRDF_{\lambda} = \frac{differential\ radiance}{differential\ irradiance} = \frac{P_s / \Omega}{P_i \cos\theta_s}$$

Stover [13] describes the scattered surface radiance as the light flux scattered per unit solid angle, Ω. The solid angle is used to refer to some small surface area on the hemisphere which has units in steradians (sr). The projected

solid angle is the solid angle multiplied by $cos(\theta_s)$ at scattering angle, θ_s. The incident surface irradiance is the incident light flux per unit illuminated surface area. It assumes a single incident beam of light and a fixed angle of incidence. The geometry of BRDF is illustrated below [14].

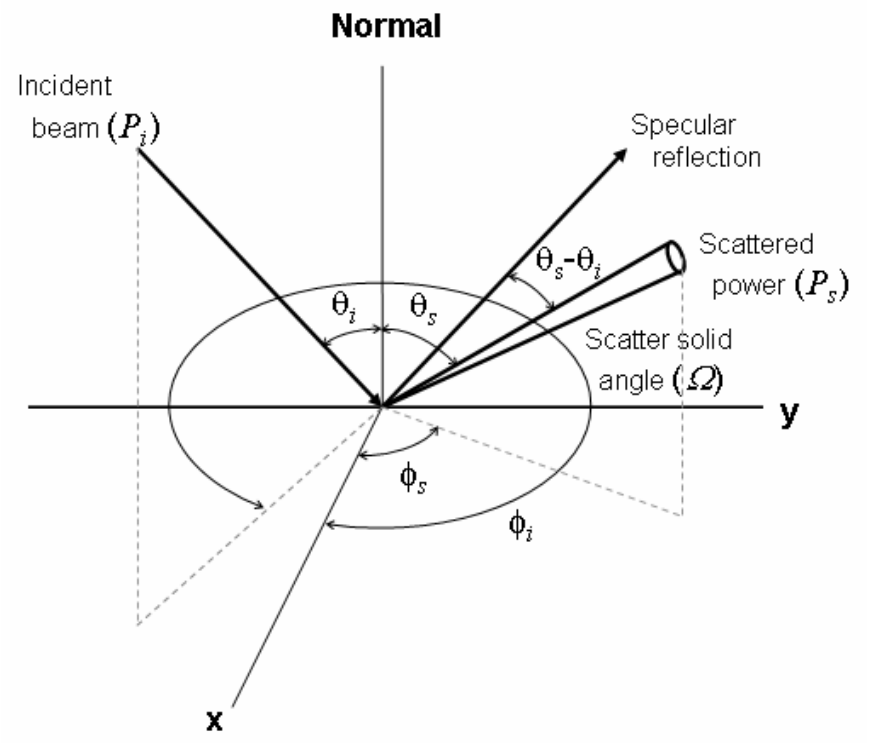

Figure 10. Definition of BRDF.

BRDF is a defined by four angles describing the direction of the incident and scattered beams using spherical coordinates. Therefore, it is common that BRDF is written as the following.

$$BRDF_\lambda\ (\theta_i, \phi_i, \theta_s, \phi_s)$$

BRDF is measured by sweeping a single detector through an arc. The incidence angle is kept constant and the angle of the detector is varied to measure the scattered intensity at different angles. It can be normalized as a probability density function (PDF) containing valuable information about the topographic features of the surface. Measurements can therefore be used to determine the size and distribution of surface features. The technique for characterizing the surface roughness of smooth, clean reflective surfaces from BRDF is well known; however, these calculations can not be used to obtain the PSD for rough surfaces. Stover [15] provides a brief explanation describing the limitations of the current analytical approaches for describing the relationship between surface topography and reflective scatter from rough surfaces.

CHAPTER THREE

EXPERIMENT PROCEDURE

Coating Composition

A generic coating was developed in order to obtain the broadest range of surface roughnesses. A simple thermoplastic resin was modified with a single pigment of varying size and concentration to obtain a desired surface roughness. In addition, the color of the initial resin was modified using a prepared carbon black dispersion to reduce volume scatter. The concentration of carbon black was set at a constant 3% for all formulations while the concentration of silica was varied. Precipitated silica is a common flatting agent used in standard camouflage coatings to reduce gloss, thus, it was selected to vary the surface roughness.

Two sizes of precipitated silica particles (Lo-Vel 27 and Lo-Vel HSF) were selected from PPG Industries, Inc. The pigments were then measured using a Beckman Coulter laser diffraction particle size analyzer. The results of 3 runs per sample were averaged to obtain a particle size of 1.57 μm for Lo-Vel 27 and 11.68 μm for Lo-Vel HSF. Appendix A has the particle size distribution of run number 1 for each pigment.

Xylene was also added to dilute the formulation to a sprayable viscosity. A spreadsheet was created to perform quick calculations of the actual amounts of formulation components required for the various pigment loadings. An example spreadsheet is illustrated in Appendix B.

Design of Experiments

A test matrix was developed using design of experiments (DOE) methodology to investigate surface roughness and is shown in Table 1. The 3 factors that were varied include particle size, pigment volume concentration, and dry film thickness. Each factor was varied at two levels resulting in 8 different formulations. The response of the DOE matrix is BRDF and surface roughness.

Table 1. A 3 factor 2 level DOE matrix.

Std. Order	Factor 1	Factor 2	Factor 3
1	-	-	-
2	+	-	-
3	-	+	-
4	+	+	-
5	-	-	+
6	+	-	+
7	-	+	+
8	+	+	+

The levels at which to vary these factors were determined using preliminary formulations. A study examining the effects of PVC on viscosity

and surface roughness was completed for each pigment in order to identify a formulation that exhibits the effect. A series of draw-downs at 1 mil thicknesses were created on Leneta cards and 3 inch x 6 inch aluminum panels. The pigment loading was increased at 2% PVC intervals. Leneta cards were used to evaluate the hiding power of the carbon black concentration to ensure an opaque surface.

The draw-downs were then visually inspected to determine the specularity of the panel. The panels were first viewed at low grazing angles using the naked eye. The specular effect was first observed at 8% PVC for the 2 micron pigment and 6% PVC for the 10 micron pigment. It was easier to identify the sudden specular effect from the 2 micron silica coatings. Based upon the visual inspection of the draw downs, three formulations were selected (Lo-Vel 27 at 4%, 6%, and 8% PVC) and sprayed on 12 inch x 12 inch panels of 0.032 inch thick aluminum to verify the presence of the effect in the visible region. The 12 inch x 12 inch panels were placed on the scatterometer and then visually inspected again. The scatterometer is capable of detecting the specular peak within a 0.10 of a degree. The effect was observed at 86 degrees angle of incidence in the visible region and 83 degrees angle of incidence in the near-infrared region for the 8% PVC loading. During this evaluation, sample flatness was found to be critical for identifying the specular component and indicated that a thicker substrate was required.

Gloss was also measured using a Gardco Novo-Gloss™ statistical glossmeter shown in Figure 11 to further establish suitable values for the PVC. Three readings were taken for each sample. The gloss data is reported in Appendix C. The resultant experiment variables are described in Table 2. The first value for the PVC was chosen based on visual inspection and the second value was chosen based on the gloss requirements to impart camouflage features (gloss @ 60° – max 5 and gloss @ 85° – max 9).

Table 2. Experiment variables.

Factor 1: Particle size
PPG precipitated silica; Lo-Vel 27, 2 μm (-) and Lo-Vel HSF, 10 μm (+)

Factor 2: Pigment volume concentration
Lo-Vel 27 8% (-) and 12 % (+)
Lo-Vel HSF 6% (-) and 10 % (+)

Factor 3: Dry film thickness
2 passes using HVLP gun (-)
4 passes using HVLP gun (+)

Figure 11. Gardco Novo-Gloss™ glossmeter.

The factors were varied according to the experiment matrix shown below.

Table 3. Experiment matrix.

Std. Order	Factor 1	Factor 2	Factor 3
1	27	8%	2 passes
2	HSF	6%	2 passes
3	27	12%	2 passes
4	HSF	10%	2 passes
5	27	8%	4 passes
6	HSF	6%	4 passes
7	27	12%	4 passes
8	HSF	10%	4 passes

Coating Application

The typical procedure for coating application is described. Panels of bare 2024-T3 aluminum were first cut into 3 inch x 6 inch pieces. Before applying the coatings, each panel was wiped with Methyl Ethyl Ketone (MEK) to remove dust and contaminants. A 12 inch x 12 inch panel of 0.125 inch thick aluminum was also cleaned for each intended formulation. The coatings were then applied using a High Volume Low Pressure (HVLP) spray gun. HVLP spray application provides a random surface texture similar to that of current camouflage coatings. Each panel was also assigned a sample identification number and a random run order was applied to the experiment

matrix before spraying. The formulation and order in which the panels were sprayed is tabulated below.

Table 4. Spray process order.

Run Order	Std. Order	Sample I.D.	Factor 1	Factor 2	Factor 3
1	2	PNT00472	HSF	6%	2 passes
2	5	PNT00463	27	8%	4 passes
3	1	PNT00475	27	8%	2 passes
4	3	PNT00473	27	12%	2 passes
5	8	PNT00471	HSF	10%	4 passes
6	4	PNT00462	HSF	10%	2 passes
7	7	PNT00474	27	12%	4 passes
8	6	PNT00461	HSF	6%	4 passes

During the spray process, all coatings were first applied using a HVLP gun. However, after examining the surface appearance of the finished panels, it was determined that some panels needed to be resprayed due to surface defects and difficulties encountered during spraying. PNT00472, PNT00462, and PNT00471 were resprayed using a gun with a larger nozzle. Table 5 identifies the process conditions for each panel. The spray equipment is noted as such the MLS gun refers to the small nozzle and the new gun refers to the large nozzle.

Table 5. Sample descriptions.

Std. Order	Sample I.D.	Particle Size	PVC	Thickness	Spray Equip.
1	PNT00475	Lo-Vel 27	8%	2 passes	MLS gun
2	PNT00472	Lo-Vel HSF	6%	2 passes	new gun
3	PNT00473	Lo-Vel 27	12%	2 passes	MLS gun
4	PNT00462	Lo-Vel HSF	10%	2 passes	new gun
5	PNT00463	Lo-Vel 27	8%	4 passes	MLS gun
6	PNT00461	Lo-Vel HSF	6%	4 passes	MLS gun
7	PNT00474	Lo-Vel 27	12%	4 passes	MLS gun
8	PNT00471	Lo-Vel HSF	10%	4 passes	new gun

Measurement Technique

BRDF measurements were obtained using a custom laser scatterometer shown in Figure 12. Samples are mounted and balanced on a spinner plate at the center of the scatter hemisphere. The spinner plate rotates at 600 revolutions per minute (RPM) spinning the sample in order to reduce noise making it easier to identify peaks from the speckle. For this particular study, 12 inch x 12 inch size panels are necessary for low grazing angles due to the enlarged spot size of the laser source.

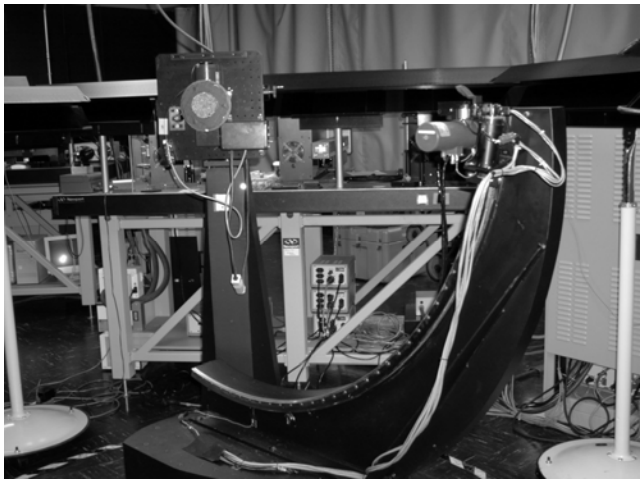

Figure 12. Scatterometer equipment.

Because the 12 inch x 12 inch panels of aluminum were so heavy, a special sample mount was designed to replace the spinner plate assembly. Figure 13 is a schematic of the spinner plate assembly. The mounts were machined to precisely duplicate the holes connecting the plate to the scatterometer. The new mounts were then permanently attached to the back of each 12 inch x 12 inch panel using epoxy.

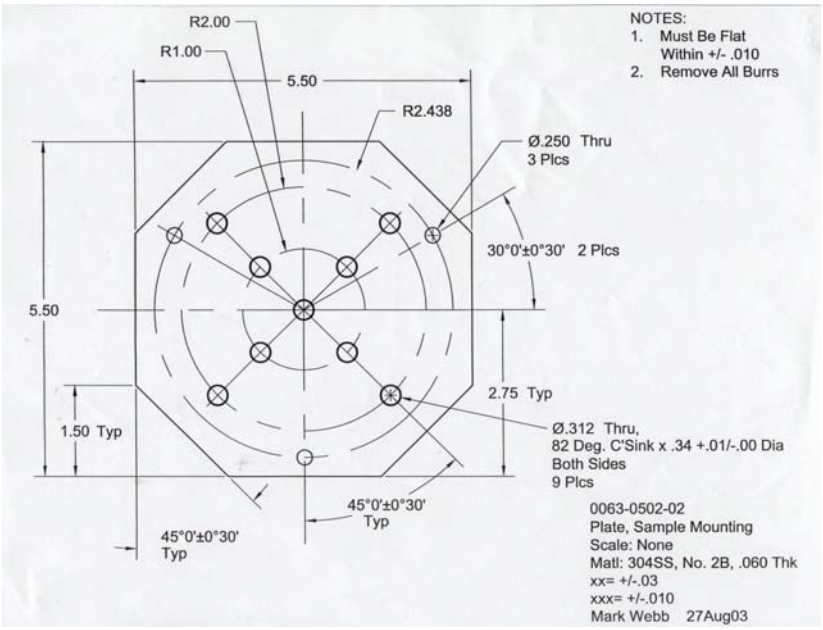

Figure 13. Spinner plate assembly.

Measurements were conducted using a HeNe gas laser producing visible light at a wavelength of 0.633 μm. The light is scattered by the sample to a receiver assembly shown in Figure 14. The receiver assembly consists of a pre-amplifier, silicon detector, and receiver polarizer. Data was collected in the plane of the receiver i.e. the incident beam and reflected beam are in-plane with the receiver. Both *s*- and *p*- polarized radiation was measured to determine the effect of polarization states. The *s*- indicates that the electric field is perpendicular to the plane of incidence and *p*- indicates that the electric field is parallel.

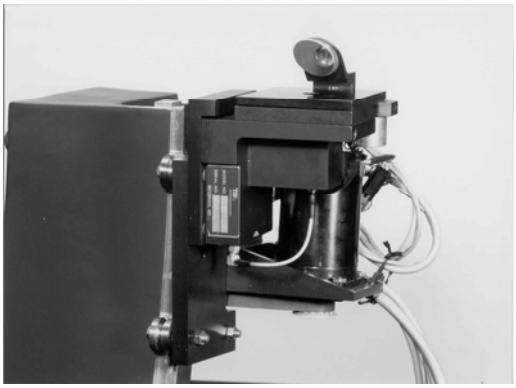

Figure 14. Receiver assembly.

Data was collected using different diameter apertures of 14 mm, 1 mm, and 0.3 mm. Smaller apertures are able to resolve peaks more clearly by restricting the amount of reflected energy at the receiver; however, decreasing the aperture size results in increased noise in the data. Therefore, the 14 mm aperture was used to provide the general shape of the curve and determine the location in which the specular peak begins to emerge from the speckle. Scans were performed at various angles of incidence to within ± 3 degrees of the specular direction of the reflected beam in search of a specular peak. The peaks initially appeared at angles greater than 82 degrees using the 14 mm aperture for the samples studied. Once the angle at which the specular peak was revealed, scans using the smaller apertures could be limited to angles surrounding 82 degrees. Thus, scans were started at 78 degrees to ensure the specular peak was captured for the samples studied. The detailed procedures for the scatterometer measurements at both *s*- and *p*- polarizations are documented in Appendix D.

Surface Roughness Evaluation

A variety of analytical techniques were evaluated to determine the appropriate method for measuring surface roughness. This includes scanning electron microscopy (SEM) stereopair imaging, atomic force microscopy (AFM), stylus and laser profilometry, and white light interferometry. Table 6 compares the advantages and disadvantages of each technique.

Table 6. Comparison of various analytical techniques to measure surface roughness [16, 17].

	Optical Profiler	**Mechanical Profiler**	**AFM**	**SEM**
Parameters measured	Surface topography	Surface topography	Surface topography	High magnification imaging
Destructive	No	No	No	Yes; requires the surface to be coated
Vertical resolution	0.1 nm	0.5 nm	0.01 nm	Not Applicable
Lateral resolution	0.35-9 μm, depending on optical system	0.1-25 μm, depending on stylus radius	0.1 nm	1-50 nm in secondary electron mode
Quantification	Yes; three-dimensional	Yes; three-dimensional	Yes; three-dimensional	Yes; using stereopair imaging software but parameters dependent upon magnification
Measurement area	8 mm x 6 mm	2 mm x 2 mm	0.5 μm x 0.5 μm	Dependent upon magnification

Using SEM stereopairs to obtain surface roughness statistics was intensely considered. SEM images of a single coated panel were captured at

varying degrees of tilt: 0, -7, and +7 degrees. The images were then combined using stereopair imaging software, Alicona MeX v4.1, to create a three-dimensional map of the surface shown in Figure 15. The software also calculated various surface parameters; however, these parameters are dependent upon magnification indicating that the value for average roughness at 250X is different than the value at 500X. Thus, these parameters can only be used for comparison purposes.

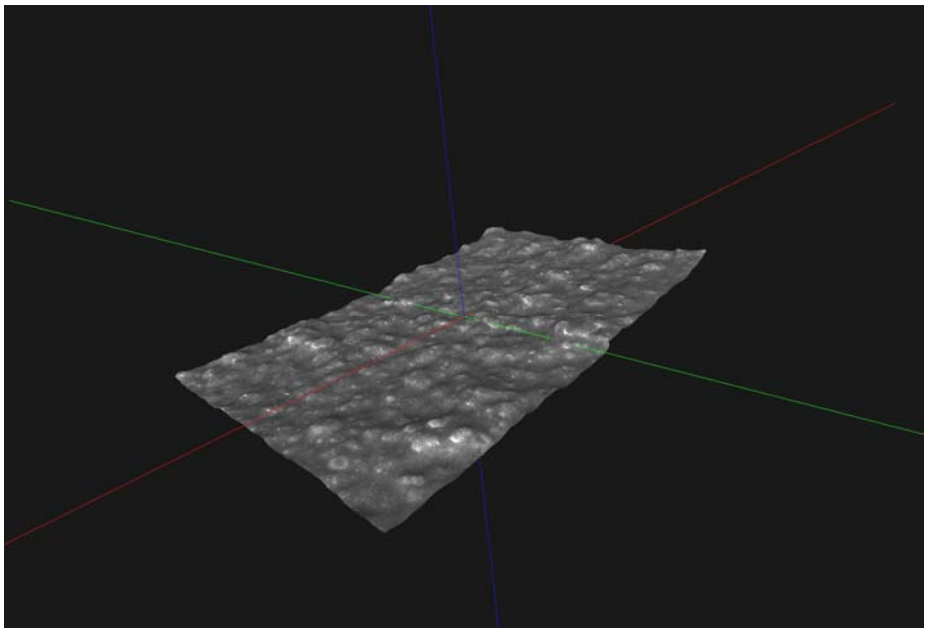

Figure 15. Three-dimensional map using stereopair imaging at 250X magnification.

Although AFM is a high resolution three-dimensional profilometer, it is limited by the small size of its measurement area. This technique would be more useful for measuring structured surfaces. Stylus and laser profilometry

are similar in that each is constrained by either the stylus radius or spot size. The stylus appeared to ignore the valleys of comparable coatings with low gloss while the laser rounded off the peaks. A significant portion of the data was missing from the two-dimensional profiles. White light interferometry was assessed next. The technique is old, but use of modern electronics such as an improved detector has enhanced its capabilities tremendously. The white light interferometer provided a couple advantages over laser, for example, the multiple wavelength operation is able to measure larger steps and generate less noise.

Therefore, surface roughness was measured using a Wyko NT1100 surface profiler shown in Figure 16. The Wyko surface profiler system is a non-contact optical profiler that uses white light interferometry to measure surface heights. Interference fringes are produced when light is reflected from a reference mirror and is combined with light reflected from the sample using a Michelson objective as illustrated in Figure 17. The NT1100 operates in two working modes: vertical shift interference (VSI) and phase shift interference (PSI). VSI mode is based on white light vertical scanning interferometry and is used to measure rough surfaces with a maximum step height of 1 mm. PSI mode measures smooth surfaces with a relatively small step height of 150 nm using phase-shifting.

Figure 16. Wyko white light interferometer.

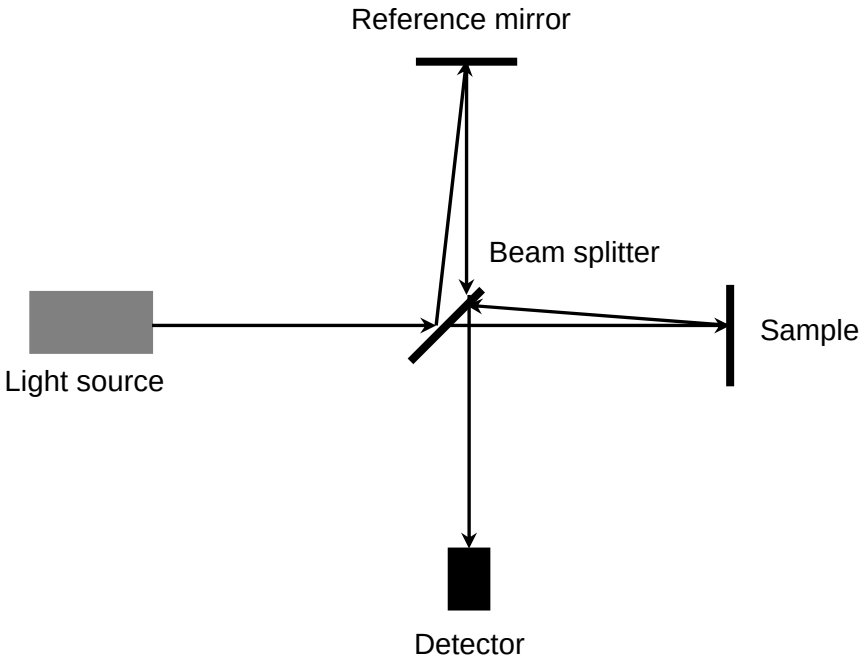

Figure 17. Setup of Michelson interferometer.

The 3 inch x 6 inch panels were measured using VSI mode using the 5X objective with a 1.0 numerical aperture resulting in a measurement area of 1.24 mm x 0.94 mm. In VSI mode, the short coherence length of white light is filtered using a neutral density filter and the interferometric objective is vertically moved to scan the surface at varying heights and the degree of fringe modulation or coherence is measured [18]. The vertical scan length was set to 15 μm x 15 μm for Lo-Vel 27 with a frequency modulation of 1% and 30 μm x 30 μm for Lo-Vel HSF with a frequency modulation of 0.1%. The modulation threshold determines the signal-to-noise level for which a given pixel is considered valid. Data points that do not meet the criteria are marked as invalid and not used during analysis. If the threshold is decreased too much, then poor quality data points are considered.

Thirty locations were measured on the surface of each 3 inch x 6 inch panel to obtain a statistical average of the surface roughness. Thirty data points are generally required to obtain a normally distributed mean. This was verified by plotting the distributions of sets of 15, 30, and 60 data points for a single coated panel. For each location, multiple measurements were combined over a 2 mm x 2 mm area using the stitching feature. The average was then calculated for various surface parameters.

CHAPTER FOUR

RESULTS AND DISCUSSION

Specular Scans using BRDF

BRDF specular scans were obtained for each panel described in the DOE experiment matrix at a wavelength of 0.633 μm from 10 to 90 degrees angles of incidence for both *s*- and *p*- polarizations. The peaks were resolved using 14 mm, 1 mm, and 0.3 mm apertures. The scans for each aperture were overlayed on a single BRDF plot as shown in Figure 18 in which specular reflection is observed at low grazing angles. An Excel macro was written to automate the process.

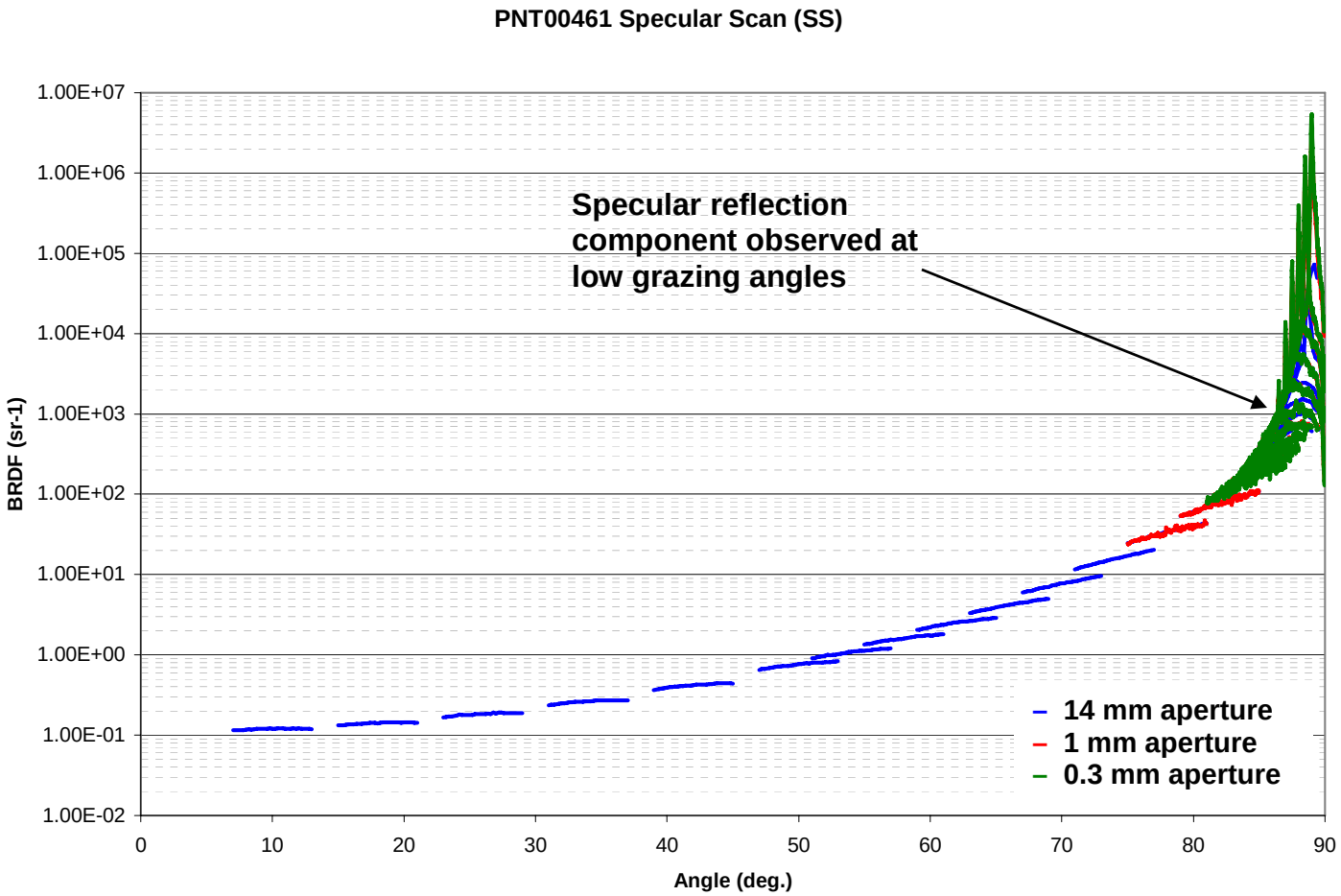

Figure 18. Specular scan using BRDF.

All of the panels measured exhibited the effect at 0.633 μm. The angle of incidence at which the specular component occurs will be referred to as the onset angle. The onset was determined for each panel by expanding the x and y scales on the graph. Figure 19 reveals an onset at 86 degrees angle of incidence for sample PNT00461.

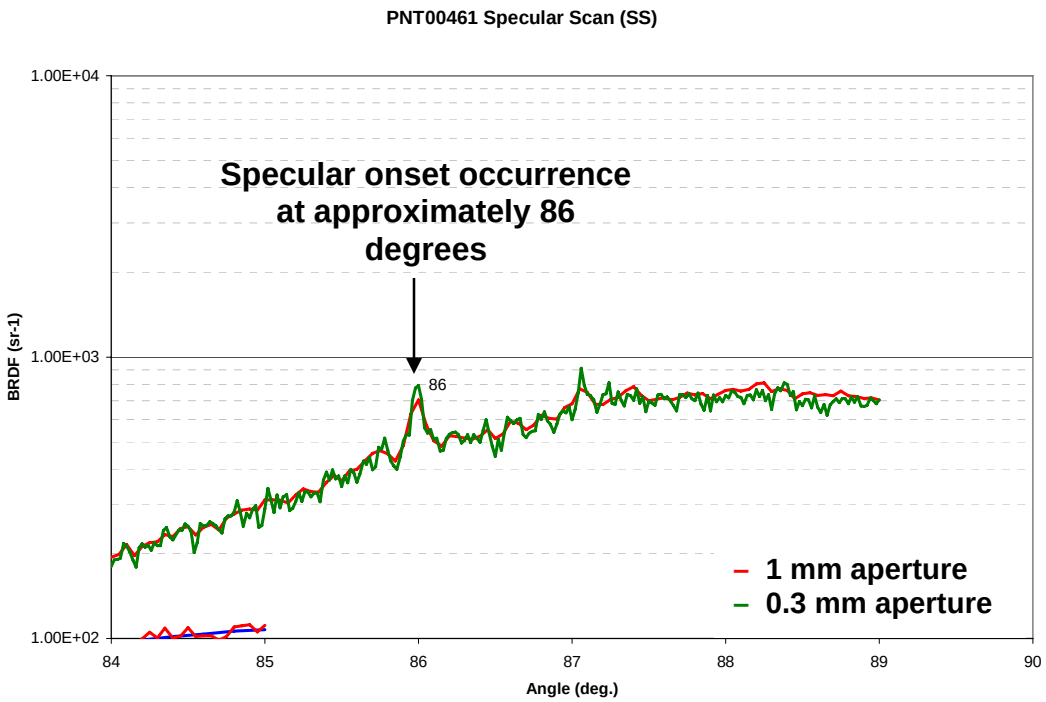

Figure 19. Onset angle.

The intensity of the specular component was also measured in order to determine the rise or growth of this effect as shown in Figure 20. The results are summarized in Table 7 where the peak intensity at onset refers to the intensity of the specular component and the base intensity at onset refers to the intensity of the diffuse or incoherent component.

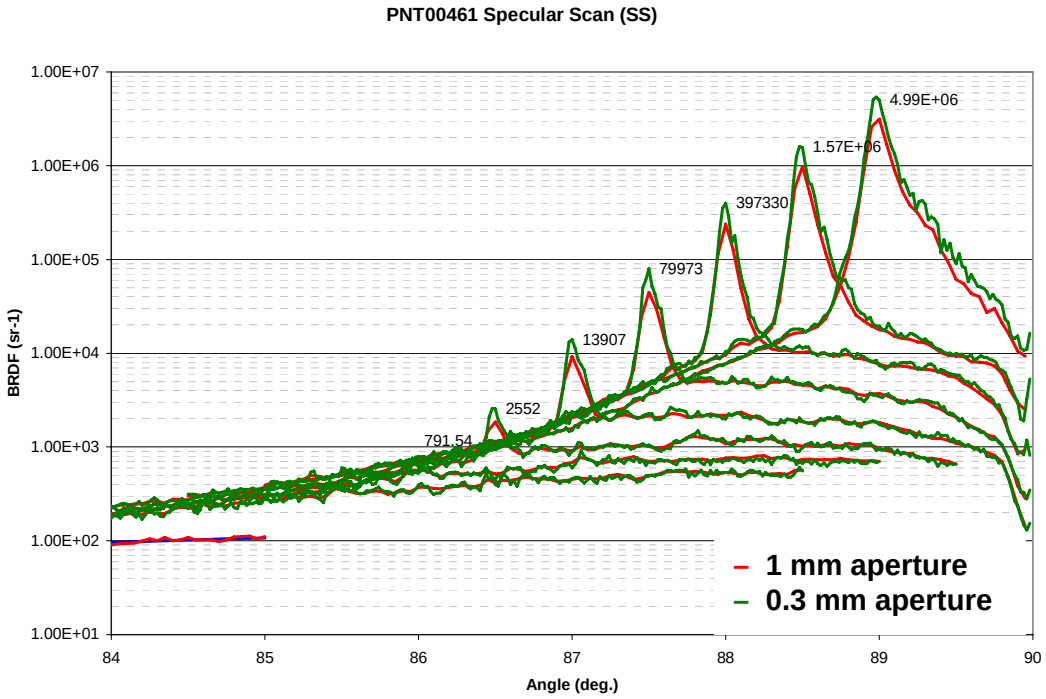

Figure 20. Intensity and growth rate.

Table 7. Onset of specular reflection using BRDF.

	Sample Description					BRDF						Surface Roughness				
Std. Order	Sample I.D.	Particle Size	PVC	Thickness	Spray Equip.	Onset angle for SSpol (deg.)	Onset angle for PPpol (deg.)	Onset angle from vis det	Peak intensity @ onset	Base intensity @ onset	Delta intensity @ onset	Average roughness, Ra (μm)	Std. Dev.	RMS roughness, Rq (μm)	Std. Dev.	Avg. Max Height, Rz (μm)
#1	PNT00475	Lo-Vel 27	8%	2 passes	MLS gun	85.5	85.5	85.2	70055	41110	28945.0	1.33	0.15	1.68	0.18	12.86
#5	PNT00463	Lo-Vel 27	8%	4 passes	MLS gun	85.5	85.5	85.4	27747	17188	10559	1.34	0.12	1.70	0.15	14.69
#3	PNT00473	Lo-Vel 27	12%	2 passes	MLS gun	86.0	86.0	85.7	12615	5074.9	7540.1	1.64	0.16	2.07	0.19	17.84
#7	PNT00474	Lo-Vel 27	12%	4 passes	MLS gun	86.0	86.0	85.9	21027	10863	10164	1.48	0.13	1.87	0.16	15.79
#2	PNT00472	Lo-Vel HSF	6%	2 passes	new gun	86.0	86.0	85.8	1089.4	482.67	606.73	2.34	0.13	2.98	0.15	56.79
#6	PNT00461	Lo-Vel HSF	6%	4 passes	MLS gun	86.0	86.0	85.8	791.54	442.65	348.89	2.38	0.07	3.04	0.10	50.43
#4	PNT00462	Lo-Vel HSF	10%	2 passes	new gun	87.0	87.0	86.9	746.19	532.76	213.43	4.28	0.16	5.52	0.19	91.59
#8	PNT00471	Lo-Vel HSF	10%	4 passes	new gun	86.5	86.5	86.6	699.17	486.23	212.94	3.02	0.16	3.91	0.20	91.84

The intensity growth rate was similar at each roughness value. A smaller particle size/smoother surface has a greater intensity at the onset which was expected. Furthermore, no polarization effects were observed. The onset angle specified for the *s*- polarization state is equal to that of the *p*-polarization for the samples studied. Multiple scatter events occurring at the surface attribute to this effect.

The onsets occurred at angles between 85 and 87 degrees for surface roughnesses ranging from 1.68 μm to 5.52 μm. The roughnesses described are root-mean-square (RMS) roughness values. RMS values are most commonly reported in literature. Figure 21 shows the relationship between incident angle and RMS surface roughness. Due to the limited range of angles, more data points were required to obtain an accurate representation of the entire curve. In order to fill in the bottom of the curve, a smoother surface is desired with a RMS surface roughness less than 1.68 μm; thus, four additional formulations were created using the Lo-Vel 27 2 μm pigment at 2%, 4%, 6%, and 8% PVC. However, a slower solvent and surface additive was used. Surface additives improve leveling and substrate wetting resulting in a smoother surface.

Table 8 describes the experiment variables for the additional formulations.

Table 8. Additional formulation descriptions.

Factor 1	Factor 2	Factor 3
27	2%	2 passes
27	4%	2 passes
27	6%	2 passes
27	8%	2 passes

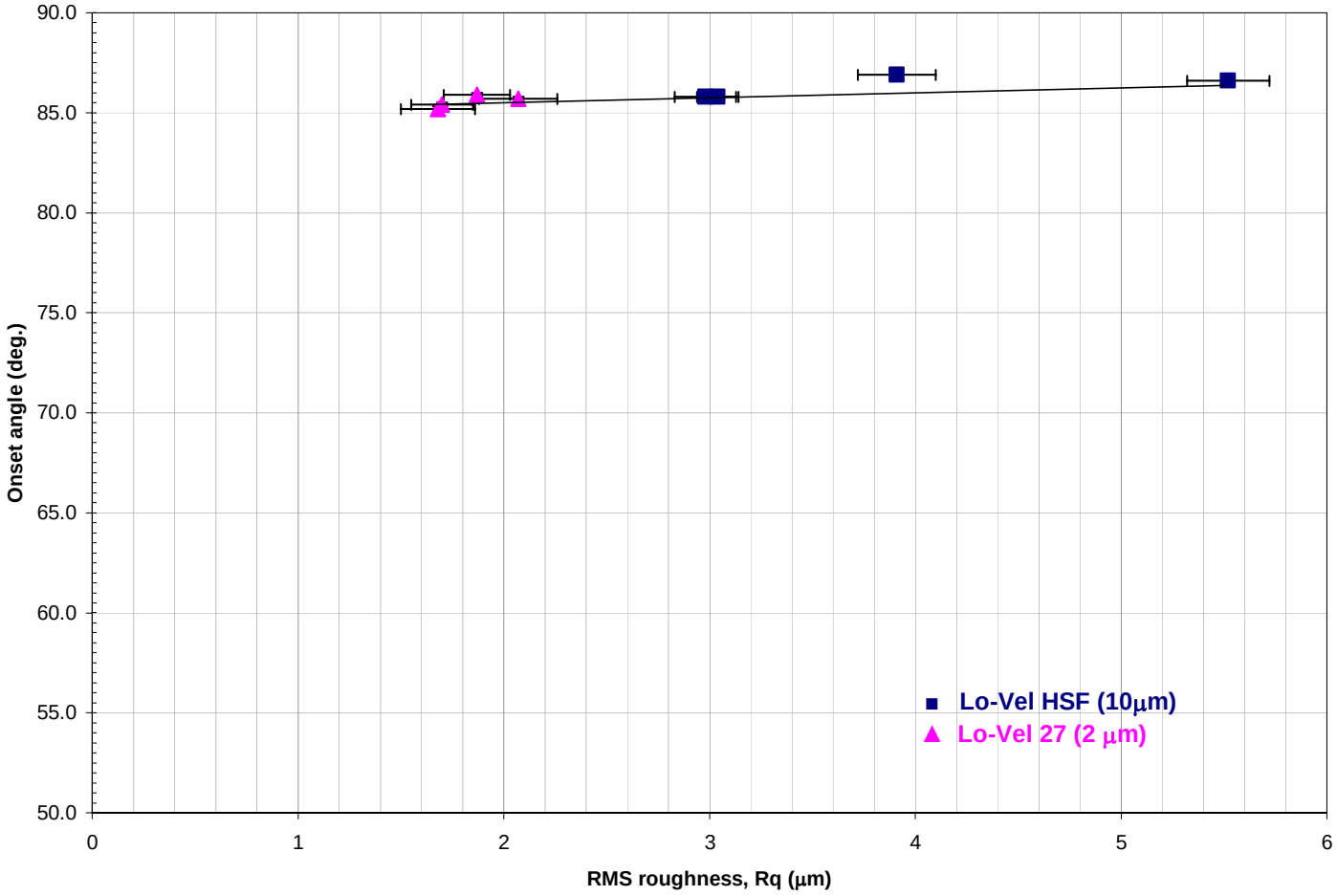

Figure 21. Effects of surface roughness and incident angle using initial set of 8 panels.

Specular scans were not collected for the additional formulations to determine the onset. Instead, the panels were visually inspected using the scatterometer. It was more difficult to identify the specular component from the speckle for these particular panels due to the smoothness of the surface. The onset angles are tabulated in Table 9.

Table 9. Measured onset angles for the additional formulations.

	Sample Description				BRDF	Surface Roughness			
Std. Order	Particle Size	PVC	Thickness	Spray Equip.	Onset angle from vis det	Average roughness, Ra (μm)	Std. Dev.	RMS roughness, Rq (μm)	Std. Dev.
#13	Lo-Vel 27	2%	2 passes	new gun	63.5	0.24	0.02	0.45	0.05
#14	Lo-Vel 27	4%	2 passes	new gun	59.5	0.36	0.04	0.57	0.08
#15	Lo-Vel 27	6%	2 passes	new gun	64.0	0.50	0.02	0.80	0.10
#16	Lo-Vel 27	8%	2 passes	new gun	69.8	0.60	0.02	0.86	0.06

Finally, the onset angle versus surface roughness has been plotted for the entire series of twelve panels. The onset angles plotted represent the angle identified from visual detection. The effects rendering a nonlinear relationship are shown in Figure 22. The primary observation from the graph is that the onset angle occurs at larger angles of incidence as surface roughness increases implying that smoother surfaces exhibit the effect sooner. In addition, the onset angle was noticed to increase with increasing PVC for a particular particle size as well as roughness. The thickness, however, does not appear to affect the onset angle. The larger particle size had the greatest onset (onset occurs later).

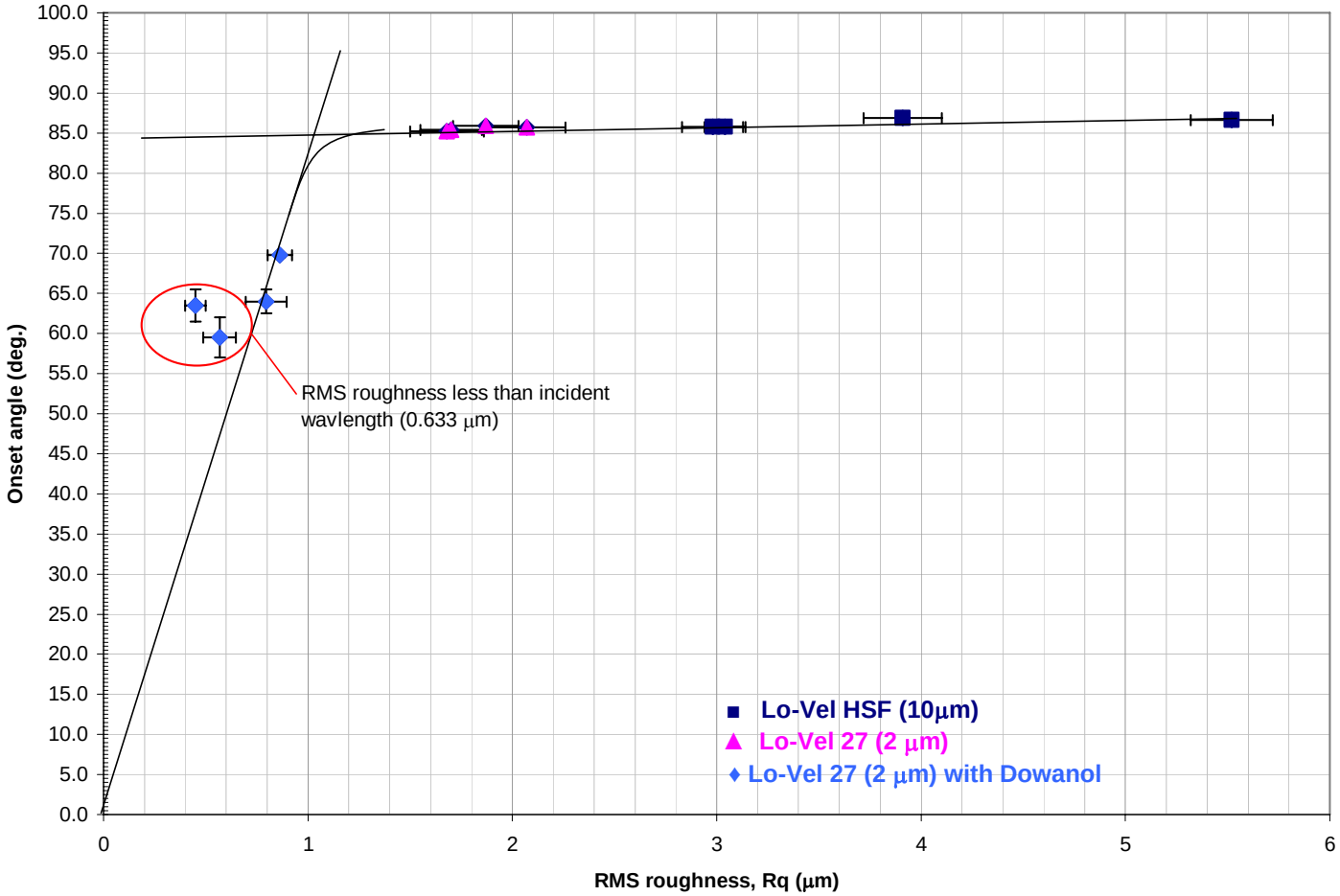

Figure 22. Effects of surface roughness and incident angle.

Trend lines were added to outline the possible shape of the curve. A sharp slope is evident for roughnesses less than 1 μm while the slope of the remaining data points increases ever so slightly. Two values have strayed from the trend line as annotated on the graph. This may be due to the RMS surface roughness being less than the incident wavelength (0.633 μm) promoting diffraction at the surface. Or this may also be due to surface texture which will be discussed in the next section. In theory, two surfaces may have the same roughness value, but have two different textures. The same type of behavior occurs for average roughness values. The only difference being that the average roughness is less than the RMS roughness for each value reported (see Table 7 and Table 9). Furthermore, it is expected that the knee in the curve would move to the right for longer wavelengths.

The behavior below 60 degrees angle of incidence is unknown. It is assumed that for very small angles of incidence the relationship again may not be linear. The resultant curve consisting of a linear portion between two nonlinear portions; however, no data was collected to support this claim.

Effects of Various Surface Roughness Parameters

The various surface parameters measured using the Wyko interferometer are listed below.

Average roughness, Ra

RMS roughness, Rq

Avg. max height, Rz

Peak-to-valley, Rt

Skewness, Rsk

Kurtosis, Rku

Autocovariance (t)

These parameters are used to describe the surface. For example, a negative skewness indicates the predominance of valleys whereas a positive skewness is present for surfaces with peaks. Kurtosis is used to explain the texture of the surface. A spiky surface area will have a high Rku > 3, bumpy surfaces have a low Rku < 3, and perfectly random surface Rku = 3. And covariance can be used to further elaborate on the randomness of a surface. A random surface generally has low correlation.

Figures 23, 24, and 25 are representative of the different surfaces using Lo-Vel 27 with Dowanol, Lo-Vel HSF, and Lo-Vel 27. A different surface texture was observed for each set of process conditions. Two of the surfaces are uniformly spiky while the remaining surface has an inherent waviness. This may be due to the change of spray equipment used. More

spikes, not necessarily larger spikes, are observed on the surface using the smaller particle size when comparing Figure 23 and Figure 24.

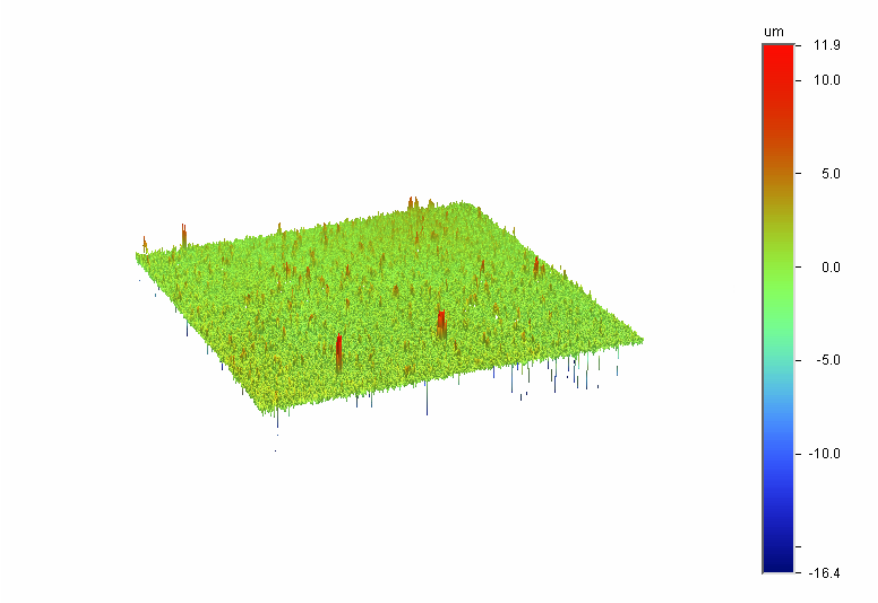

Figure 23. Three-dimensional topography of surface with Rq = 0.80 μm (Lo-Vel 27 with Dowanol, 6% PVC, 2 passes, new gun).

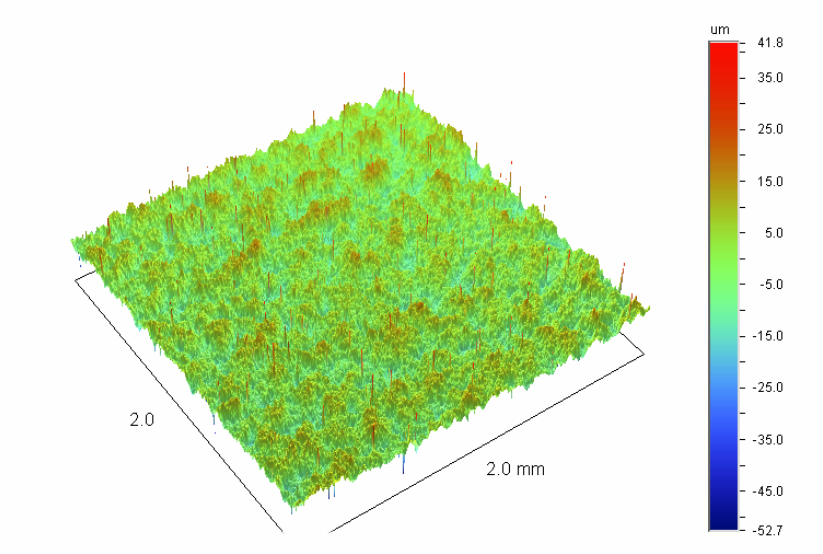

Figure 24. Three-dimensional topography of surface with Rq = 5.52 μm (Lo-Vel HSF, 10% PVC, 2 passes, new gun).

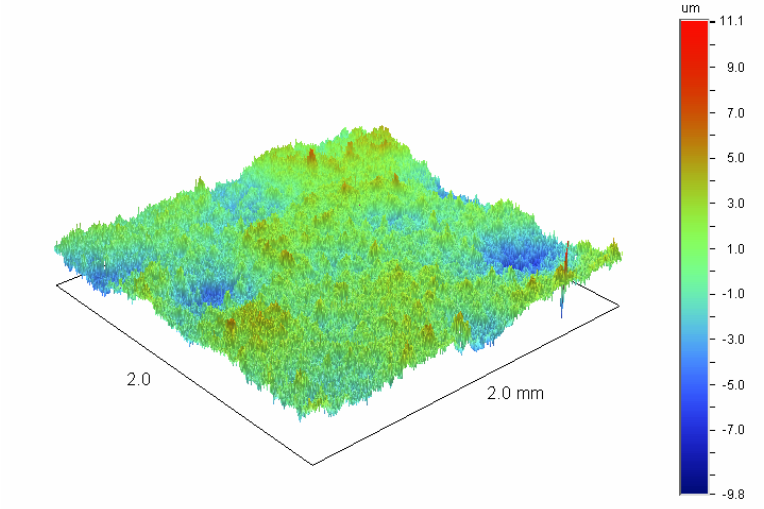

Figure 25. Three-dimensional topography of surface with Rq = 1.70 μm (Lo-Vel 27, 8% PVC, 4 passes, MLS gun).

The covariance was also examined for each set of process conditions. The covariance is a measure of the correlation properties of the surface's roughness and is used to study the relationship between two data sets. If the surface is periodic the resulting autocovariance will also be periodic. A surface with periodic features shows higher correlation. The following figures represent the autocovariance function for each set of process conditions.

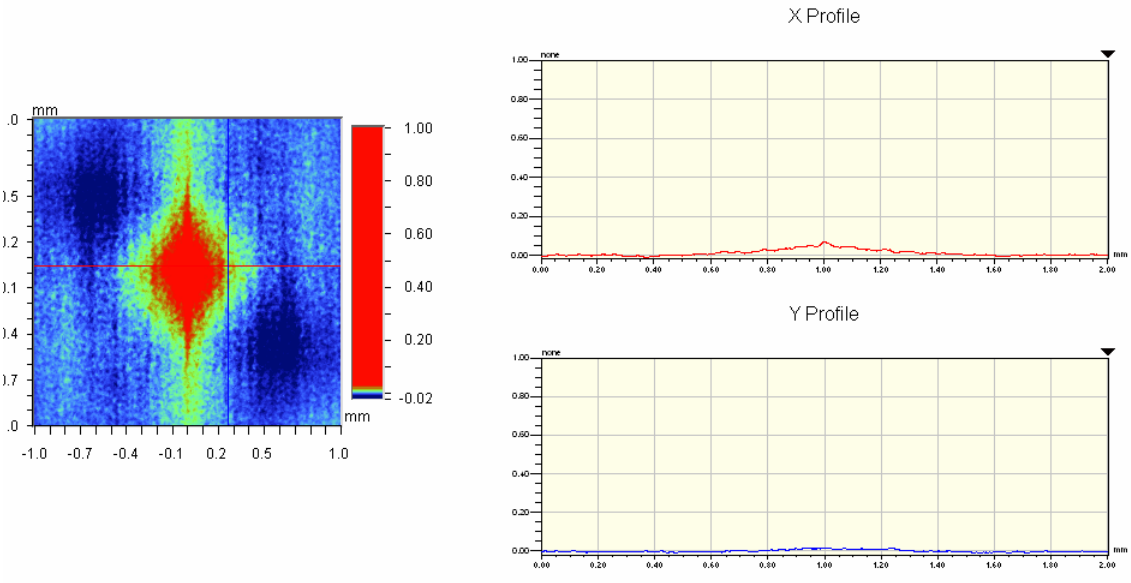

Figure 26. Autocovariance function of surface with Rq = 0.57 μm (Lo-Vel 27 with Dowanol, 4% PVC, 2 passes, new gun).

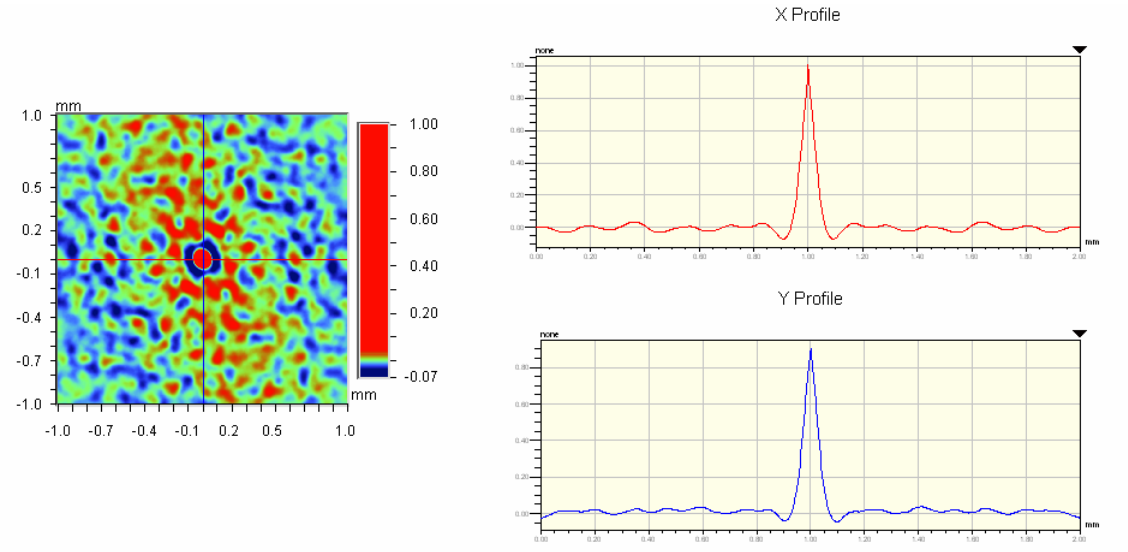

Figure 27. Autocovariance function of surface with Rq = 2.98 μm (Lo-Vel HSF, 6% PVC, 2 passes, new gun).

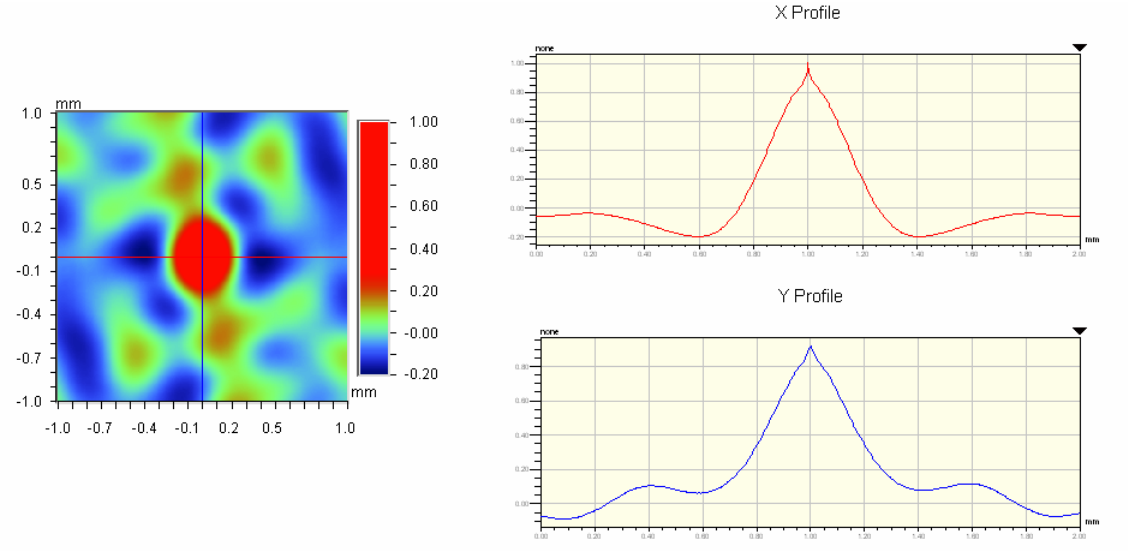

Figure 28. Autocovariance function of surface with Rq = 1.68 μm (Lo-Vel 27, 8% PVC, 2 passes, MLS gun).

The PVC did not appear to affect the correlation properties of the rough surfaces obtained using Lo-Vel 27 and Lo-Vel HSF; however, the set of smoother surfaces using Lo-Vel 27 with Dowanol showed some sensitivity to PVC. From the autocovariance functions, the larger particle has a more random surface meaning the surface feature is less likely to repeat itself. Overall, more correlation was observed at 4 passes versus 2 passes for each set of processing conditions. This is most likely due to pigment settling that occurs in thicker coatings. Surface roughness data is reported in Appendix E. After thorough examination of the surface parameters, no one surface property contributed solely to the occurrence of the specular component.

CHAPTER FIVE

SUMMARY AND CONCLUSION

Various rough surfaces have been characterized using BRDF to reveal a specular peak in the visible region. Specular peaks were identified for RMS roughnesses ranging between 1.68 μm and 5.52 μm. The angle at which this specular component becomes visible changes depending on the surface roughness, the rougher the surface the greater the angle of incidence. A combination of surface roughness and randomness of the surface was determined to contribute to this effect. Surface roughness was perceived to affect the onset angle whereas randomness was perceived to affect the intensity of the specular peak.

Camouflage coatings require a gloss less than 5 gloss units at 60 degrees of incidence and less than 9 gloss units at 85 degrees. Generic coatings meeting the requirement produced this effect at angles greater than 86 degrees. To visually detect an aircraft at grazing angles implies that the distance between the object and the observer is very large; thus, negating the requirement to manage reflection at these angles. Furthermore, solar glint is minimized at these angles because the reflection is concentrated at a narrow

viewing angle making visual tracking difficult [19]. So, does the coating require a gloss less than 9? And could the gloss requirement be increased to 12, for example, to allow specular behavior at grazing angles and improve durability? Decreasing the PVC by 4%, increases the onset angle only by 1 to 1.5 degrees. An area of concern would then be to understand the effects of wavelength for a particular surface roughness. A very rough surface that is not specular to visible light possibly will be to infrared radiation. Further investigation is required to follow the occurrence of the specular effect at various wavelengths for a single surface roughness.

The other issue discussed with regards to the gloss requirement is the gloss measurement itself. The requirements specified for camouflage coatings lie in the nonlinear portion of the measurement range at 60 degrees and the behavior is unknown for values less than 10 at 85 degrees. The results become questionable within these ranges, therefore, suggests that gloss is not the proper tool for evaluating scatter from camouflage coatings. However, gloss is an easy and portable measurement technique that can be used in the field.

Accurate interpretation of the reflectance properties of a material requires the knowledge of BRDF. It is the width of the BRDF peak that is affected by the surface roughness and/or gloss as commonly reported in literature; however, glossmeters measure the intensity of specular reflection which is associated with the magnitude of the BRDF peak. This may contribute to the inconsistencies experienced in gloss measurements. Of

equal concern is that gloss values may be artificial because of the presence of this specular effect meaning that the gloss requirement was based on a measurement value that was over specular. Hence, camouflage coatings are being over specified by using gloss as the requirement. Perhaps surface roughness could be used as a requirement. A roughness of at least 0.86 μm is required to reach angles greater than 70 degrees according to the data collected.

Ultimately, BRDF should be specified and the measurement should be obtained at angles associated with certain threat conditions. By using BRDF, the specular behavior of low gloss coatings was thoroughly examined in the visible region wherein a specular peak was observed at grazing angles of incidence. Specular behavior was also observed at 3.39 μm and 10.6 μm in which the initial occurrence of the specular peak appeared at smaller angles of incidence and varied as a function of wavelength. This effect has not been previously documented in literature. The understanding of this behavior will guide the development of future camouflage coatings. In addition, the presence of a specular peak in the visible region can be explored to debate image formation in rough surfaces and may be used to explain the mirages that are formed when the conditions for the total internal reflection are not satisfied as described by Tavassoly et. al. [20].

Appendix A – Particle Size Distribution Data

BECKMAN COULTER

LS Particle Size Analyzer

26 Mar 2005

File name:	Lo Vel 2.$01	Group ID:	Lo Vel 27
Sample ID:	Lo Vel 27		
Run number:	1	Operator:	Lisa Farrier
Comments:	2 micron silica		
Optical model:	Silica.rfd PIDS included		
LS 230	Small Volume Module		
Start time:	2:03 26 Mar 2005	Run length:	91 seconds
Obscuration:	6%	PIDS Obscur:	55%
Fluid:	Water		
Sample Density:	2.2 g/mL		
Software:	3.01	Firmware:	2.02 0

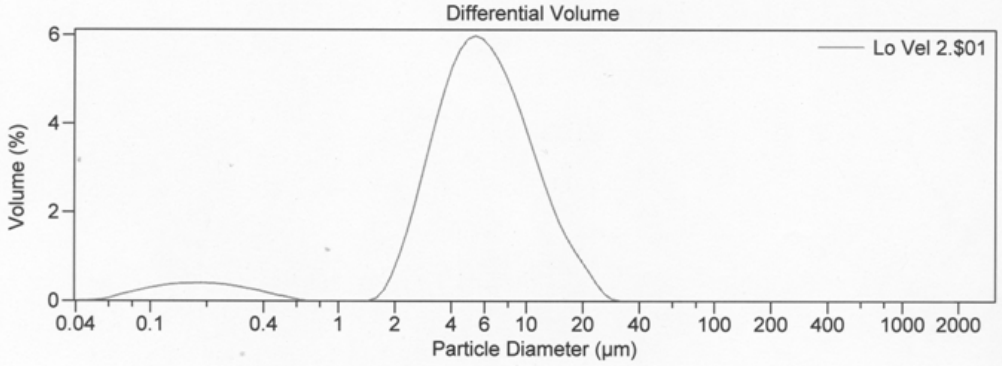

Volume Statistics (Arithmetic) Lo Vel 2.$01

Calculations from 0.0400 µm to 2000 µm

Volume:	100%		
Mean:	6.568 µm	S.D.:	4.400 µm
Median:	5.563 µm	C.V.:	67.0%
D(3,2):	1.621 µm	Skewness:	1.316 Right skewed
Mode:	5.354 µm	Kurtosis:	2.335 Leptokurtic

% <	10	25	50	75	90
µm	2.385	3.669	5.563	8.527	12.44

BECKMAN COULTER

LS Particle Size Analyzer

26 Mar 2005

File name:	Lo Vel H.$01	Group ID:	Lo Vel HSF
Sample ID:	Lo Vel HSF		
Run number:	1	Operator:	Lisa Farrier
Comments:	10 micron silica		
Optical model:	Silica.rfd PIDS included		
LS 230	Small Volume Module		
Start time:	1:48 26 Mar 2005	Run length:	92 seconds
Obscuration:	21%	PIDS Obscur:	48%
Fluid:	Water		
Sample Density:	2.2 g/mL		
Software:	3.01	Firmware:	2.02 0

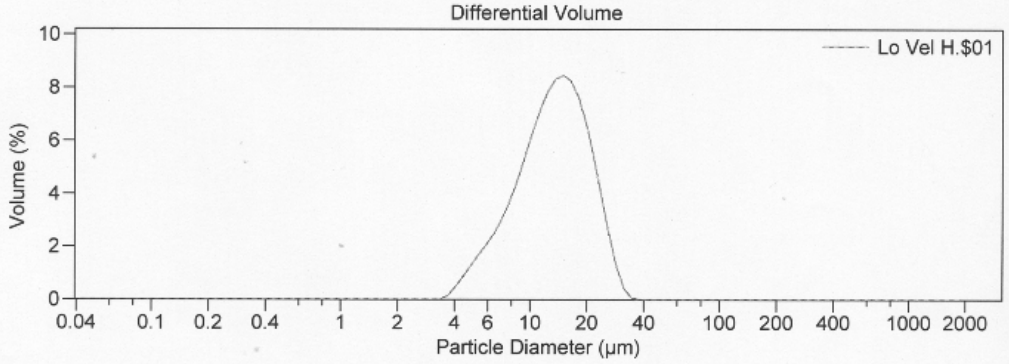

Volume Statistics (Arithmetic) Lo Vel H.$01

Calculations from 0.0400 µm to 2000 µm

Volume:	100%		
Mean:	14.08 µm	S.D.:	5.705 µm
Median:	13.47 µm	C.V.:	40.5%
D(3,2):	11.67 µm	Skewness:	0.506 Right skewed
Mode:	14.94 µm	Kurtosis:	-0.206 Platykurtic

% <	10	25	50	75	90
µm	6.976	9.732	13.47	17.86	22.08

Appendix B – Formulation Spreadsheet

Flatting Agent Dispersion

	Mass (g)	Sub-Component	Component	Density (g/cm^3)	Mass (g)	Wt. Frac.
PPG Lo-Vel 27	**8.00**	n/a	Pigment	2.100	8.00	0.13
Xylene	**28.00**	n/a	Solvent	0.860	28.00	0.44
SIA QC4820	**28.00**					
		Polyester urethane	Resin	1.100	7.56	0.12
		Solvent Mixture	Solvent	0.900	20.44	0.32
					64.00	1.00

TINT-AYD ST 8317 (Black Pigment Dispersion)

	Component	Density (g/cm^3)	Mass (g)	Wt. Frac.
Carbon Black	Pigment	1.800	0.28	0.28
Acrylic Resin	Resin	1.100	0.30	0.30
PM Acetate	Solvent	0.960	0.42	0.42
			1.00	1.00

SIA QC4820 (Polymer Solution)

	Component	Density (g/cm^3)	Mass (g)	Wt. Frac.
Polyester urethane	Resin	1.100	0.27	0.27
Solvent Mixture	Solvent	0.900	0.73	0.73
			1.00	1.00

Dilution Solvent

	Component	Density (g/cm^3)
Xylene	Solvent	0.860

	Desired Values				
Formula Number	Lo-Vel 27 PVC	Carbon Black PVC	NVV	Total Vol. (mL)	Dry Vol. (cm3)
LF-27-0	**0.00**	**0.03**	**0.190**	**12.5**	2.375
LF-27-1	**0.02**	**0.03**	**0.190**	**12.5**	2.375
LF-27-2	**0.04**	**0.03**	**0.190**	**12.5**	2.375
LF-27-3	**0.06**	**0.03**	**0.190**	**12.5**	2.375
LF-27-4	**0.08**	**0.03**	**0.190**	**12.5**	2.375
LF-27-5	**0.10**	**0.03**	**0.190**	**12.5**	2.375
LF-27-6	**0.12**	**0.03**	**0.190**	**12.5**	2.375
LF-27-7	**0.14**	**0.03**	**0.190**	**12.5**	2.375
LF-27-8	**0.16**	**0.03**	**0.190**	**12.5**	2.375
LF-27-9	**0.18**	**0.03**	**0.190**	**12.5**	2.375
LF-27-10	**0.20**	**0.03**	**0.190**	**12.5**	2.375

	Flatting Agent (cm3)	Flatting Agent (g)	Flatting Agent Dispersion (g)	Carbon Black (cm3)	Carbon Black (g)	TINT-AYD ST 8317 (g)	Total Resin (cm3)	Existing Resin (cm3)	Resin Needed (cm3)	SIA QC4820 (g)	Existing Solvent (cm3)	Solvent Needed (cm3)	Xylene (g)
	0.000	0.000	0.00	0.07125	0.12825	0.46	2.30375	0.125	2.179	8.88	7.400	2.725	2.34
	0.048	0.100	0.80	0.07125	0.12825	0.46	2.25625	0.211	2.046	8.33	7.649	2.476	2.13
	0.095	0.200	1.60	0.07125	0.12825	0.46	2.20875	0.296	1.912	7.79	7.898	2.227	1.91
	0.143	0.299	2.39	0.07125	0.12825	0.46	2.16125	0.382	1.779	7.25	8.147	1.978	1.70
	0.190	0.399	3.19	0.07125	0.12825	0.46	2.11375	0.468	1.646	6.71	8.396	1.729	1.49
	0.238	0.499	3.99	0.07125	0.12825	0.46	2.06625	0.553	1.513	6.16	8.645	1.480	1.27
	0.285	0.599	4.79	0.07125	0.12825	0.46	2.01875	0.639	1.380	5.62	8.894	1.231	1.06
	0.333	0.698	5.59	0.07125	0.12825	0.46	1.97125	0.725	1.246	5.08	9.143	0.982	0.84
	0.380	0.798	6.38	0.07125	0.12825	0.46	1.92375	0.810	1.113	4.54	9.392	0.733	0.63
	0.428	0.898	7.18	0.07125	0.12825	0.46	1.87625	0.896	0.980	3.99	9.641	0.484	0.42
	0.475	0.998	7.98	0.07125	0.12825	0.46	1.82875	0.982	0.847	3.45	9.890	0.235	0.20

	27 Dispersion (g)	Tint-Ayd (g)	SIA (g)	Xylene (g)	27 (cm3)	CB (cm3)	Resin (cm3)	Solvent (cm3)	27 PVC	CB PVC	NVV
LF-27-0	**0.00**	**0.46**	**8.88**	**2.34**	0.000	0.071	2.304	10.125	0.000	0.030	0.190
LF-27-1	**0.80**	**0.46**	**8.33**	**2.13**	0.048	0.071	2.256	10.125	0.020	0.030	0.190
LF-27-2	**1.60**	**0.46**	**7.79**	**1.91**	0.095	0.071	2.209	10.125	0.040	0.030	0.190
LF-27-3	**2.39**	**0.46**	**7.25**	**1.70**	0.143	0.071	2.161	10.125	0.060	0.030	0.190
LF-27-4	**3.19**	**0.46**	**6.71**	**1.49**	0.190	0.071	2.114	10.125	0.080	0.030	0.190
LF-27-5	**3.99**	**0.46**	**6.16**	**1.27**	0.238	0.071	2.066	10.125	0.100	0.030	0.190
LF-27-6	**4.79**	**0.46**	**5.62**	**1.06**	0.285	0.071	2.019	10.125	0.120	0.030	0.190
LF-27-7	**5.59**	**0.46**	**5.08**	**0.84**	0.333	0.071	1.971	10.125	0.140	0.030	0.190
LF-27-8	**6.38**	**0.46**	**4.54**	**0.63**	0.380	0.071	1.924	10.125	0.160	0.030	0.190
LF-27-9	**7.18**	**0.46**	**3.99**	**0.42**	0.428	0.071	1.876	10.125	0.180	0.030	0.190
LF-27-10	**7.98**	**0.46**	**3.45**	**0.20**	0.475	0.071	1.829	10.125	0.200	0.030	0.190

Appendix C – Gloss Data

Sample Description			85 deg. Gloss				60 deg. Gloss			
Formula Number	Particle Size	PVC	Run1	Run2	Run3	**Average**	Run1	Run2	Run3	**Average**
LF-27-0	Lo-Vel 27	0%	94.6	94.8	94.6	**94.7**	89.5	89.2	89.4	**89.4**
LF-27-1	Lo-Vel 27	2%	33.6	32.7	32.5	**32.9**	37.6	37.8	37.8	**37.7**
LF-27-2	Lo-Vel 27	4%	28.8	28.6	28.6	**28.7**	28.8	29.2	29.2	**29.1**
LF-27-3	Lo-Vel 27	6%	33.7	31.9	31.2	**32.3**	25.1	23.9	24.8	**24.6**
LF-27-4	Lo-Vel 27	8%	25.0	24.3	23.8	**24.4**	15.2	14.9	14.5	**14.9**
LF-27-5	Lo-Vel 27	10%	13.6	14.9	14.4	**14.3**	7.4	7.2	7.7	**7.4**
LF-27-6	Lo-Vel 27	12%	9.0	9.9	9.7	**9.5**	3.4	3.5	4.1	**3.7**
LF-27-7	Lo-Vel 27	14%	9.6	10.3	10.2	**10.0**	2.6	2.6	2.5	**2.6**
LF-27-8	Lo-Vel 27	16%	8.3	8.7	8.5	**8.5**	1.3	1.3	1.4	**1.3**
LF-27-9	Lo-Vel 27	18%	6.5	6.2	6.2	**6.3**	0.6	0.5	0.5	**0.5**
LF-27-10	Lo-Vel 27	20%	4.9	4.2	4.3	**4.5**	0.4	0.4	0.4	**0.4**
LF-HSF-0	Lo-Vel HSF	0%	80.5	79.3	81.0	**80.3**	82.5	82.4	81.5	**82.1**
LF-HSF-1	Lo-Vel HSF	2%	38.2	40.4	36.1	**38.2**	46.2	48.5	43.8	**46.2**
LF-HSF-2	Lo-Vel HSF	4%	18.9	21.2	16.7	**18.9**	24.3	26.5	26.5	**25.8**
LF-HSF-3	Lo-Vel HSF	6%	9.0	7.4	10.4	**8.9**	12.6	12.9	12.6	**12.7**
LF-HSF-4	Lo-Vel HSF	8%	4.3	5.3	3.8	**4.5**	6.8	7.0	6.7	**6.8**
LF-HSF-5	Lo-Vel HSF	10%	2.0	2.1	1.9	**2.0**	3.0	3.1	3.0	**3.0**
LF-HSF-6	Lo-Vel HSF	12%	1.5	1.7	1.3	**1.5**	1.6	1.6	1.7	**1.6**
LF-HSF-7	Lo-Vel HSF	14%	1.1	1.1	1.2	**1.1**	0.8	0.9	0.9	**0.9**
LF-HSF-8	Lo-Vel HSF	16%	1.0	1.0	1.0	**1.0**	0.6	0.6	0.6	**0.6**
LF-HSF-9	Lo-Vel HSF	18%	0.9	0.9	0.9	**0.9**	0.3	0.3	0.3	**0.3**
LF-HSF-10	Lo-Vel HSF	20%	NA	NA	NA		NA	NA	NA	

Appendix D - Procedure for Scatterometer Measurements

SS Polarization:

- Set source and receiver polarizers to 90°.
- Move sample theta to an angle large enough for the specular peak to appear (Usually 87°-88°).
- Remove precession from sample.
- Set sample theta to 50° and increase sample theta in increments of 1° until specular peak emerges from speckle. Specular scan will begin with beta chosen from the set (50°, 54°, 58°, 62°, 66°, 70°, 74°, 78°) whichever value is closest to and less than the sample theta value at which the specular peak emerges.
- Run power scans.
- Run specular scan for the 14 mm aperture for entire range of sample theta values.
- Insert 1 mm aperture.
- Find locations of beta and alpha stages for peak power at the angle at which the specular peak is clear. (Usually 87°-88°)
- Reconfigure positions of beta and alpha.
- Run specular scan for the 1 mm aperture beginning at sample theta value used for aperture calibration.
- Insert 0.3 mm aperture.
- Find locations of beta and alpha stages for peak power at the angle at which the specular peak appears. (Usually 87°-88°)
- Reconfigure positions of beta and alpha.
- Run specular scan for the 0.3 mm aperture beginning at sample theta value used for aperture calibration.
- Run power scans.
- Scan definition files:
  - 14 mm aperture: SPCDFSSH.SDF (Data file extension *.sdh)
    Full range for sample theta, beta ± 3°, step 0.2°
  - 1 mm aperture: SPCDFSSM.SDF (Data file extension *.sdm)
    Sample theta dependent on onset of specularity, beta ± 3°, step 0.05°
  - 0.3 mm aperture: SPCDFSSS.SDF (Data file extension *.sds)
    Sample theta dependent on onset of specularity, beta ± 3°, step 0.02°

PP Polarization:

- Set source and receiver polarizers to 0°.
- Move sample theta to an angle large enough for the specular peak to appear (Usually 87°-88°).
- Remove precession from sample.
- Set sample theta to 50° and increase sample theta in increments of 1° until specular peak emerges from speckle. Specular scan will begin with beta chosen from the set (50°, 54°, 58°, 62°, 66°, 70°, 74°, 78°) whichever value is closest to and less than the sample theta value at which the specular peak emerges.
- Run power scans.
- Run specular scan for the 14 mm aperture for entire range of sample theta values.
- Insert 1 mm aperture.
- Find locations of beta and alpha stages for peak power at the angle at which the specular peak appears. (Usually 87°-88°)
- Reconfigure positions of beta and alpha.
- Run specular scan for the 1 mm aperture beginning at sample theta value used for aperture calibration.
- Insert 0.3 mm aperture.
- Find locations of beta and alpha stages for peak power at the angle at which the specular peak appears. (Usually 87°-88°)
- Reconfigure positions of beta and alpha.
- Run specular scan for the 0.3 mm aperture beginning at sample theta value used for aperture calibration.
- Run power scans.
- Scan definition files:
  - 14 mm aperture: SPCDFPPH.SDF (Data file extension *.pdh)
    Full range for sample theta, beta ± 3°, step 0.2°
  - 1 mm aperture: SPCDFPPM.SDF (Data file extension *.pdm)
    Sample theta dependent on onset of specularity, beta ± 3°, step 0.05°
  - 0.3 mm aperture: SPCDFPPS.SDF (Data file extension *.pds)
    Sample theta dependent on onset of specularity, beta ± 3°, step 0.02°

Appendix E – Surface Roughness Data

	Sample Description				Surface Roughness							
Std. Order	Particle Size	PVC	Thickness	Spray Equip.	Average roughness, Ra (μm)	Std. Dev.	RMS roughness, Rq (μm)	Std. Dev.	Avg. Max Height, Rz (μm)	Peak-to-valley (μm)	Skewness, Rsk	Kurtosis, Rku
#1	Lo-Vel 27	8%	2 passes	MLS gun	1.33	0.15	1.68	0.18	12.86	16.12	-0.21	3.14
#2	Lo-Vel HSF	6%	2 passes	new gun	2.34	0.13	2.98	0.15	56.79	61.32	0.51	4.43
#3	Lo-Vel 27	12%	2 passes	MLS gun	1.64	0.16	2.07	0.19	17.84	21.06	-0.23	3.15
#4	Lo-Vel HSF	10%	2 passes	new gun	4.28	0.16	5.52	0.19	91.59	94.97	-0.29	7.24
#5	Lo-Vel 27	8%	4 passes	MLS gun	1.34	0.12	1.70	0.15	14.69	18.14	0.06	3.54
#6	Lo-Vel HSF	6%	4 passes	MLS gun	2.38	0.07	3.04	0.10	50.43	59.69	0.32	4.48
#7	Lo-Vel 27	12%	4 passes	MLS gun	1.48	0.13	1.87	0.16	15.79	18.70	-0.17	3.23
#8	Lo-Vel HSF	10%	4 passes	new gun	3.02	0.16	3.91	0.20	91.84	101.26	-0.27	9.57
#13	Lo-Vel 27	2%	2 passes	new gun	0.24	0.02	0.45	0.05	25.02	28.85	-10.55	429.87
#14	Lo-Vel 27	4%	2 passes	new gun	0.36	0.04	0.57	0.08	25.92	30.64	-3.19	151.5
#15	Lo-Vel 27	6%	2 passes	new gun	0.50	0.02	0.80	0.10	25.92	28.53	-2.73	70.09
#16	Lo-Vel 27	8%	2 passes	new gun	0.60	0.02	0.86	0.06	26.74	29.23	-0.36	29.64

References

1. Federal Standard 595 Paint Specification – Colors used in government procurement, FED-STD-595 B, 11 January 1994.

2. Z. Wicks, et al. Organic coatings: Science and Technology. 2nd Ed., John Wiley & Sons, New York (1999).

3. U.S. Military Specification – Polyurethane coatings for aircraft and support equipment, MIL-PRF-85285C (AS), 30 April 1997.

4. Available at http://profc.udec.cl/~gabriel/tutoriales/rsnote/contents.htm, accessed August 2006.

5. J. Stover. Optical Scattering: Measurements and Analysis. 2nd Ed., SPIE Optical Engineering Press, Washington D. C. (1995).

6. Available at http://en.wikipedia.org/wiki/Gloss_(material_appearance), accessed August 2006.

7. J. Johnson. Advanced Coating Systems for Aircraft Corrosion Protection. Presentation. SERDP Partners in Environmental Technology. (2001).

8. J. Johnson. Computer Assisted Coatings Design: CPVC Issues. Ph.D. Thesis, Chemistry Department, North Dakota State University, North Dakota (2000).

9. ASTM Standard D523 – Standard test method for specular gloss, 1999.

10. Available at http://www.coleparmer.com, accessed August 2006.

11. J. Arney, L. Ye, and S. Banach. Interpretation of Gloss Meter Measurements. submitted to J. Imag. Sci. & Technol. (2005).

12. F. Nicodemus. Reflectance Nonmenclature and Directional Reflectance and Emissivity. Appl. Opt., vol. **9**, pp. 1474-1475 (1970).

13. J. Stover. Optical Scattering: Measurements and Analysis. McGraw-Hill, New York (1990).

14. Available at http://www.schmitt-ind.com/pdf/scatter1.pdf, accessed August 2006.

15. J. Stover and M. Bernt. Measurement and Analysis of Scatter from Rough Surfaces. SPIE Stray Rad. in Opt. Syst. III, vol. **2260**, pp. 40-49 (1994).

16. J. Bennett. Recent Developments in Surface Roughness Characterization. Meas. Sci. Technol., vol. **3**, pp. 1119-1127 (1992).

17. C. Bruncle, C. Evans, and S. Wilson. Encyclopedia of Materials Characterization. Reed Publishing, Connecticut (1992).

18. C. Lamb and M. Zecchino. Wyko Surface Profilers Technical Reference Manual. version 2.2.1, Veeco Metrology Group (1999).

19. M. Tavassoly, A. Nahal, and Z. Ebadi. Image Formation in Rough Surfaces. Opt. Comm., vol. **238**, pp. 252-260 (2004).

20. C. Warner. Implementing Joint Vision 2010: A Revolution in Military Affairs for Strategic Air Campaigns. Air University Press. Maxwell AFB, Alabama (1999).

LIST OF ABBREVIATIONS

PVC	Pigment Volume Concentration
BRDF	Bidirectional Reflectance Distribution Function
PDF	Probability Density Function
DOE	Design of Experiments
ASTM	American Society of Testing and Materials
MEK	Methyl Ethyl Ketone
HVLP	High Volume Low Pressure
RPM	Revolutions Per Minute
SEM	Scanning Electron Microscopy
AFM	Atomic Force Microscopy
VSI	Vertical Scanning Interferometry
PSI	Phase Shifting Interferometry
RMS	Root Mean Square